

LA-UR-12-24533

Approved for public release; distribution is unlimited.

Title: Fission Matrix Capability for MCNP Monte Carlo

Author(s): Carney, Sean E.
Brown, Forrest B.
Kiedrowski, Brian C.
Martin, William R.

Intended for: MCNP reference documentation
Report
Web



Disclaimer:

Los Alamos National Laboratory, an affirmative action/equal opportunity employer, is operated by the Los Alamos National Security, LLC for the National Nuclear Security Administration of the U.S. Department of Energy under contract DE-AC52-06NA25396. By approving this article, the publisher recognizes that the U.S. Government retains nonexclusive, royalty-free license to publish or reproduce the published form of this contribution, or to allow others to do so, for U.S. Government purposes. Los Alamos National Laboratory requests that the publisher identify this article as work performed under the auspices of the U.S. Department of Energy. Los Alamos National Laboratory strongly supports academic freedom and a researcher's right to publish; as an institution, however, the Laboratory does not endorse the viewpoint of a publication or guarantee its technical correctness.

Fission Matrix Capability for MCNP Monte Carlo

S. E. Carney, F. B. Brown*, B. C. Kiedrowski*, W. R. Martin

The University of Michigan–Ann Arbor
Department of Nuclear Engineering & Radiological Sciences
2355 Bonisteel Boulevard, Ann Arbor, MI 48109, USA
seanec@umich.edu, wrm@umich.edu

*Los Alamos National Laboratory
X-Computational Physics Division, Monte Carlo Codes Group
P.O. Box 1663, MS A143
Los Alamos, NM 87545, USA
fbrown@lanl.gov, bckiedro@lanl.gov

August 2012

Abstract

Monte Carlo criticality calculations can be subject to slow fission source convergence for large or weakly coupled problems. By tallying the spatially-discretized fission kernel (the linear operator stochastically applied during power iteration), a low-order fundamental eigenvector is calculated to accelerate fission source convergence. In MCNP the fission matrix is stored efficiently using a sparse structure, the tallying of which requires little extra work. In addition, higher eigenmodes and eigenvalues from the fission matrix are calculated, which conventional Monte Carlo is unable to produce. After testing this method on several realistic problems, significant convergence acceleration was found, along with higher eigenmode information.

Introduction

In a Monte Carlo criticality calculation, before the tallying of quantities can begin, a converged fission source (the fundamental eigenvector of the fission kernel) is required. Tallies of interest may include powers, absorption rates, leakage rates, or the multiplication factor (the fundamental eigenvalue of the fission kernel, k_{eff}). Just as in the power iteration method of linear algebra, if the dominance ratio (the ratio of the first and zeroth eigenvalues) is high, many iterations of neutron history simulations are required to isolate the fundamental mode of the problem. Optically large systems have large dominance ratios, and systems containing poor neutron communication between regions are also slow to converge. The fission matrix method, implemented into MCNP[1], addresses these problems.

When Monte Carlo random walk from a source is executed, the fission kernel is stochastically applied to the source. Random numbers are used for: distances to collision, reaction types, scattering physics, fission reactions, etc. This method is used because the fission kernel is a complex, 7-dimensional operator that is not explicitly known. Deterministic methods use approximations/discretization in energy, space, and direction to the kernel. Consequently, they are faster. Monte Carlo directly simulates the physics, which necessitates the use of random sampling. Because of this statistical noise, common convergence acceleration methods used in deterministic methods do not work.

In the fission matrix method, we are using the random walk information not only to build the next-iteration fission source, but also a spatially-averaged fission kernel. Just like in deterministic methods, this involves approximation and discretization. The approximation is the tallying of the spatially-discretized fission kernel with an incorrect fission source. We address this by making the spatial mesh fine enough that this error is negligible. As a consequence of discretization we get a spatially low-order kernel, the fundamental eigenvector of which should converge faster than that of continuous kernel. We can then redistribute the fission bank to match the fundamental fission matrix eigenvector, effectively eliminating all higher modes. For all computations here biasing is not used, with the intention of comparing the unaltered, conventional Monte Carlo process with the fission matrix results.

The source convergence of standard Monte Carlo criticality calculations are, to some extent, always subject to the characteristics of the problem. This method seeks to partially eliminate this problem-dependence by directly calculating the spatial coupling. The primary cost of this, which has prevented widespread use since its inception [2,3,4], is the extra storage required. To account for the coupling of all N spatial regions to every other region requires storing N^2 values. For realistic problems, where a fine resolution is required for the suppression of discretization error, the storage becomes inordinate. Two factors lead to a renewed interest here: the larger memory available on modern computers and the development of a better storage scheme based on physical intuition. When the distance between source and fission events is short compared with the size of the entire system, saving memory by accounting for only local coupling introduces little extra error.

We can gain other information from directly tallying the fission kernel: higher eigenmodes and eigenvalues. Conventional Monte Carlo cannot calculate this data— here we have a way to get new information for multiplying systems. In Ref. [5], higher mode eigenfunctions are analyzed for a three-region 1-dimensional problem and 2-dimensional homogenous problem. We analyze higher modes for more realistic problems. There is also the question of practical use of this information; here we examine a

way of using eigenmode information to address the negative confidence interval bias due to inter-cycle correlation.

We apply this method mainly to four problems: 2D pressurized water reactor (PWR) [6], 3D Kord Smith Challenge [7], OECD – Nuclear Energy Agency (NEA) source convergence benchmark fuel storage vault [8], and Advanced Test Reactor (ATR) [9]. We see excellent source convergence acceleration for the most difficult problems: the 3D Kord Smith Challenge and fuel storage vault. Additionally, we examine higher eigenmode results for all these problems. Using part of the eigenvalue spectrum for a one-group 1D problem, we find confidence interval correction factors that are improvements over existing corrections [10].

Theory

The eigenvalue problem for a multiplying system is the following:

$$FS = KS \Rightarrow S_i = \frac{1}{K} \sum_{j=1}^N F_{i,j} S_j ,$$

where F is a transition matrix of fission rates, the spatially-continuous form of which is stochastically applied during Monte Carlo. The fundamental eigenpair is K and S , and N is the number of spatial regions. Element $[i,j]$ of the fission matrix F is the number of fission neutrons produced in destination region i due to an average neutron produced in origin region j . The spatial regions must be disjoint and encompass all fissionable material of the physical problem. Here we introduce operator notation for the fission matrix numerator and denominator,

$$F [i, j] = \frac{\int_0^\infty \int_0^\infty dE dE' \int_{Z_i} d^3 r \int_{Z_j} d^3 r' f(\bar{r}', E' \rightarrow \bar{r}, E) s(\bar{r}') \chi(\bar{r}', E')}{\int_0^\infty dE' \int_{Z_j} d^3 r' s(\bar{r}') \chi(\bar{r}', E')} = \frac{F_N s(\bar{r})}{F_D s(\bar{r})} ,$$

$$= \frac{\text{fission rate in spatial region } i \text{ due to fission source in cell } j}{\text{fission source in region } j} ,$$

$$= \text{fission rate in spatial region } i \text{ due to average neutron born in region } j .$$

$$f(\bar{r}', E' \rightarrow \bar{r}, E) = \text{fission kernel} = \text{neutrons produced at } (\bar{r}, E) \text{ due to a neutron at } (\bar{r}', E') ,$$

$$f(\bar{r}', E' \rightarrow \bar{r}, E) = G(\bar{r}, E; \bar{r}', E') \nu \Sigma_f(\bar{r}, E) = \text{Green's function} \cdot \text{destination fission cross section} ,$$

$$s(\bar{r}') = \text{spatial distribution of fission source} ,$$

$$\chi(\bar{r}', E') = \text{fission emission spectrum} ,$$

$$Z_j = \text{origin region} ,$$

$Z_i = \text{destination region} .$

A short derivation and discussion of the adjoint fission matrix is presented in Refs. 11 and 12.

By tallying this quantity during a Monte Carlo criticality calculation, we are discretizing the fission kernel. Error arises because the source distribution used to tally the fission matrix is not the exact source. To quantify this discretization error we use the integral mean value theorem,

$$F [i, j] = \frac{s(\bar{r} \in Z_j) \int_0^\infty \int_0^\infty dE dE' \int_{Z_i} d^3 r \int_{Z_j} d^3 r' f(\bar{r}', E' \rightarrow \bar{r}, E) \chi(\bar{r}', E')}{s(\bar{r} \in Z_j) \int_0^\infty dE' \int_{Z_j} d^3 r' \chi(\bar{r}', E')},$$

which says a fission matrix element tallied from a flat source in its origin region has a multiplicative error associated with it, equal to some ratio of true source magnitudes in the origin region. If the origin region is infinitesimal, this ratio is unity and no error is introduced for any source choice.

There are two opposing effects on accuracy that govern the choice of mesh size: sampling and discretization error. If not for the latter, an optimum fission bank biasing scheme could be devised where the fission matrix is adaptively coarsened based on confidence intervals of tallied elements.

To further quantify this error, we introduce the stochastic source to which the fission kernel is applied during Monte Carlo,

$$\hat{s}(\bar{r}) = s(\bar{r}) + \hat{\varepsilon}(\bar{r}),$$

$$E[\hat{\varepsilon}(\bar{r})] = 0,$$

and the tallied fission matrix (for one cycle),

$$\begin{aligned} \hat{F} [i, j] &= \frac{\int_0^\infty \int_0^\infty dE dE' \int_{Z_i} d^3 r \int_{Z_j} d^3 r' f(\bar{r}', E' \rightarrow \bar{r}, E) [s(\bar{r}) + \hat{\varepsilon}(\bar{r})] \chi(\bar{r}', E')}{\int_0^\infty dE' \int_{Z_j} d^3 r' [s(\bar{r}) + \hat{\varepsilon}(\bar{r})] \chi(\bar{r}', E')} = \frac{F_N s(\bar{r}) + F_N \hat{\varepsilon}(\bar{r})}{F_D s(\bar{r}) + F_D \hat{\varepsilon}(\bar{r})} \\ &= \frac{F_N s(\bar{r})}{F_D s(\bar{r})} \frac{1 + \frac{F_N \hat{\varepsilon}(\bar{r})}{F_N s(\bar{r})}}{1 + \frac{F_D \hat{\varepsilon}(\bar{r})}{F_D s(\bar{r})}} = \frac{F_N s(\bar{r})}{F_D s(\bar{r})} \left[1 + \frac{F_N \hat{\varepsilon}(\bar{r})}{F_N s(\bar{r})} \right] \left[1 - \frac{F_D \hat{\varepsilon}(\bar{r})}{F_D s(\bar{r})} + \dots \right] \approx \frac{F_N s(\bar{r})}{F_D s(\bar{r})} \left[\frac{F_N \hat{\varepsilon}(\bar{r})}{F_N s(\bar{r})} - \frac{F_D \hat{\varepsilon}(\bar{r})}{F_D s(\bar{r})} \right]. \end{aligned}$$

To first order the relative error is,

$$\frac{\hat{F} [i, j] - F [i, j]}{F [i, j]} \approx \frac{F_N \hat{\varepsilon}(\bar{r})}{F_N s(\bar{r})} - \frac{F_D \hat{\varepsilon}(\bar{r})}{F_D s(\bar{r})}.$$

Integration of the noise terms over volume has some cancellation effect. Applying the integral mean value theorem gives,

$$\frac{\hat{F}[i, j] - F[i, j]}{F[i, j]} \approx \frac{\hat{\epsilon}(\bar{r}^{\epsilon} Z_j)}{s(\bar{r}^{\epsilon} Z_j)} - \frac{\hat{\epsilon}(\bar{r}^{\prime\epsilon} Z_j)}{s(\bar{r}^{\prime\epsilon} Z_j)}.$$

Again, an origin region with an infinitesimal volume results in a fission matrix element with no discretization error.

Recognizing that each element is tallied cumulatively from successive fission banks of cycles $m=1..M$,

$$\hat{F}[i, j] = \frac{F_N s(\bar{r}) + \frac{1}{M} F_N \left[\sum_{m=1}^M \hat{\epsilon}_m(\bar{r}) \right]}{F_D s(\bar{r}) + \frac{1}{M} F_D \left[\sum_{m=1}^M \hat{\epsilon}_m(\bar{r}) \right]}.$$

Then the relative error to first order is,

$$\frac{\hat{F}[i, j] - F[i, j]}{F[i, j]} \approx \frac{\frac{1}{M} F_N \left[\sum_{m=1}^M \hat{\epsilon}_m(\bar{r}) \right]}{F_N s(\bar{r})} - \frac{\frac{1}{M} F_D \left[\sum_{m=1}^M \hat{\epsilon}_m(\bar{r}) \right]}{F_D s(\bar{r})}.$$

Fission Matrix Statistics

Others have tallied the fission matrix with the standard reaction rate tallying methods (track length, collision, absorption) [13,14,15,16]. Here, we tally by looking at the fission bank between cycles. While this method gives fewer samples, it comes with almost no additional cost.

There is no easy statistical treatment of the fission matrix. While others [13] have looked at variances of fission matrix elements and their relation to the eigen solutions, fission matrix tallies are subject to the same correlation problems of regular Monte Carlo power iteration calculations. Additionally, there is no known analytic way to find the resulting variance of the eigen solutions. Ref. [13] has found that conservative confidence interval estimates of k_{eff} can be calculated by getting the fundamental eigenvalues of fission matrices with each elements' standard deviation added and subtracted. The 68% confidence intervals they estimated in this manner are observed to be more than 90% in actuality, hence the conservatism of the estimate. Ref. [14] estimated confidence intervals by solving fission matrices sampled from an estimated normal distribution, and evaluating the resulting distribution of the fundamental eigenpair. The statistics of the fission matrix are not of primary importance, though, if the main goal is source convergence acceleration. The easiest way to judge certainty of the fission matrix estimate is to evaluate the convergence of the eigenpairs, which we do here.

Sparse Matrix Algorithm

Fig. 1 shows the fission matrix structure for a 2D Pressurized Water Reactor (PWR) model, with a 15x15x1 spatial mesh (one region per assembly). On the left is the full matrix, and on the right is the sparse matrix. The outermost bands on the left matrix correspond to fissions that occur far away from the origin region in the y-direction. For any given band, the individual bands on each edge correspond to fissions that occur far away from the origin region in the x-direction. Only ~0.5% of fissions occur more than two assembly lengths away from the origin region, which are designated nonlocal fissions. Thus, there are 5 y-bands each containing 5 x-bands in the sparse matrix. The spaces in each band correspond to non-fissionable regions, the peripheral water in this case.

Using a sparse matrix complicates two tasks in the source module: tallying the spatial bin location in the fission matrix numerator and performing the power iteration solve. No longer can we perform a simple spatial bin search for each new fission site—the bin index must be altered to fit into the sparse scheme. Additionally, nonlocal fissions must be handled.

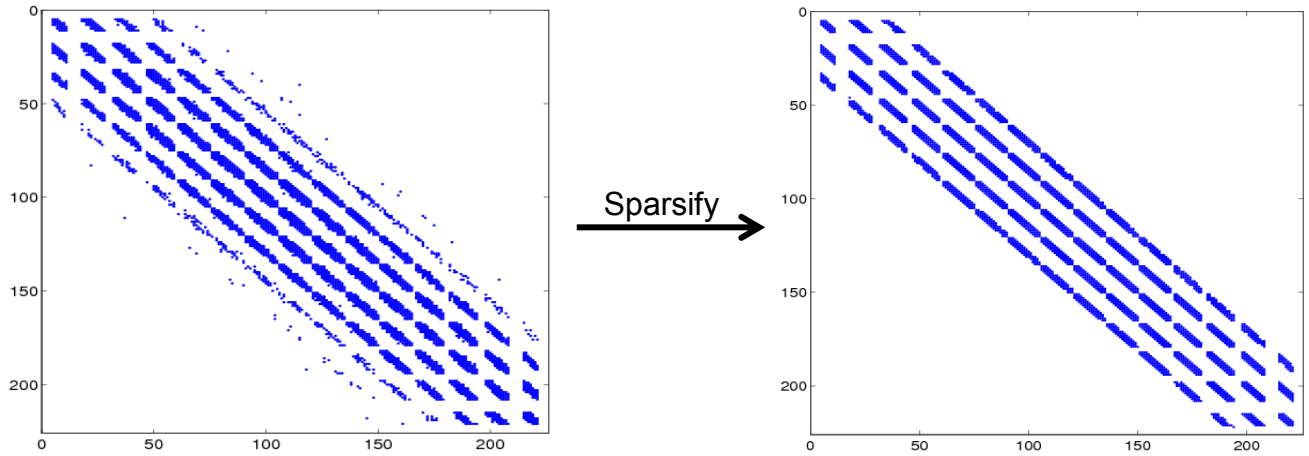


Fig. 1. Fission matrix structure for a 2D whole-core PWR model, for a 15x15x1 spatial mesh. Matrix dimension are 225 x 225. Nonzero elements are in blue.

The sparse scheme is based on geometric intuition. Instead of allocating $N \times N$ elements (N being the number of spatial bins in the problem), the sparse matrix allocates $W \times N$, where W is the number of spatial bins in the local region. The local region is the volume around region j where fissions are considered. The origin region indexing is identical to the full scheme:

$$j = n_x + (n_y - 1)N_x + (n_z - 1)N_x N_y ,$$

where

$$n_x, n_y, n_z = \text{origin indices}$$

and

$$1 \leq n_x \leq N_x ; 1 \leq n_y \leq N_y ; 1 \leq n_z \leq N_z ,$$

$$1 \leq j \leq N = N_x N_y N_z .$$

The i indexing is based on the j index:

$$i = \left(m_x - n_x + \frac{W_x + 1}{2} \right) + \left(m_y - n_y + \frac{W_y + 1}{2} - 1 \right) W_x + \left(m_z - n_z + \frac{W_z + 1}{2} - 1 \right) W_x W_y ,$$

where

$$m_x, m_y, m_z = \text{destination indices} ,$$

and

$$1 \leq m_x \leq N_x ; 1 \leq m_y \leq N_y ; 1 \leq m_z \leq N_z ,$$

$$W_x, W_y, W_z = \text{local region widths} ,$$

$$1 \leq W_x \leq 2N_x - 1 ; 1 \leq W_y \leq 2N_y - 1 ; 1 \leq W_z \leq 2N_z - 1 ,$$

$$1 \leq i \leq W = W_x W_y W_z .$$

Local region widths are always odd numbers, since each local region is centered on its origin region. A more flexible region is possible, but not currently implemented. Furthermore, in the current implementation all region widths must be equal. Note this scheme wastes memory—when the origin region is near problem boundaries, part of its local region is outside the problem and stored as zeros (this unused allocation becomes negligible for larger problems). This consideration is significant, though, when the local region covers close to the whole problem. In such a case it is possible for the sparse scheme to require more storage than the full scheme.

From the above expressions we get the fractional memory savings for matrix storage:

$$\text{fractional memory savings} = \frac{WN}{N^2} = \frac{W_x W_y W_z}{N_x N_y N_z} = \frac{\text{local region size}}{\text{problem size}}$$

As savings is fractional, for a fixed physical local region size (two assembly lengths, for example), sparse storage asymptotically approaches $O(N^2)$ storage scaling. Sparsifying is most advantageous for 3D problems. In terms of neutronics, sparsifying is ideal for large, lightly-coupled systems wherein most fissions occur locally. Such is true for PWRs. Generally speaking, the higher the dominance ratio of a problem, the larger the potential memory savings from sparsifying.

The efficacy of distance-based sparsifying weakens when region-averaged cross sections vary largely from region to region, such as near a streaming path. The alternative storage method is, for a given origin

region, to build a vector of indices of destination regions. This guarantees no fissions are lost, but makes truncating difficult.

Below is pseudocode for the tallying of the fission matrix (after the initial stage, wherein only the fission matrix denominator is tallied), which is performed in between cycles:

```
cycle though fission bank
  get saved origin region bin index
  if local fission or full storage scheme
    find destination bin index according to fission site coordinates
  elseif sparse storage scheme & nonlocal fission
    change destination to edge of local region, in fissionable region closest to actual
    destination
  end
  add final weight of previous cycle to matrix numerator with origin and destination indices
  add starting weight of next cycle to matrix denominator with true destination indices
  store spatial bin of true destination in fission bank
end
```

Eigen decomposition is also complicated with the sparse scheme. To multiply the sparse fission matrix by a vector, for each origin region (matrix column), local region regions are cycled through (moving down the column) in a stencil-like manner, and multiplications are performed.

Results

2D PWR Problem

The first realistic problem we test with is a 2D PWR [6], illustrated in Fig. 2. The core has 192 fuel assemblies of three different enrichments: 2.1%, 2.6%, and 3.1%. Each assembly is modeled as a 17x17 lattice of fuel pins and water tubes. ENDF/B-VII continuous-energy cross section data is used.

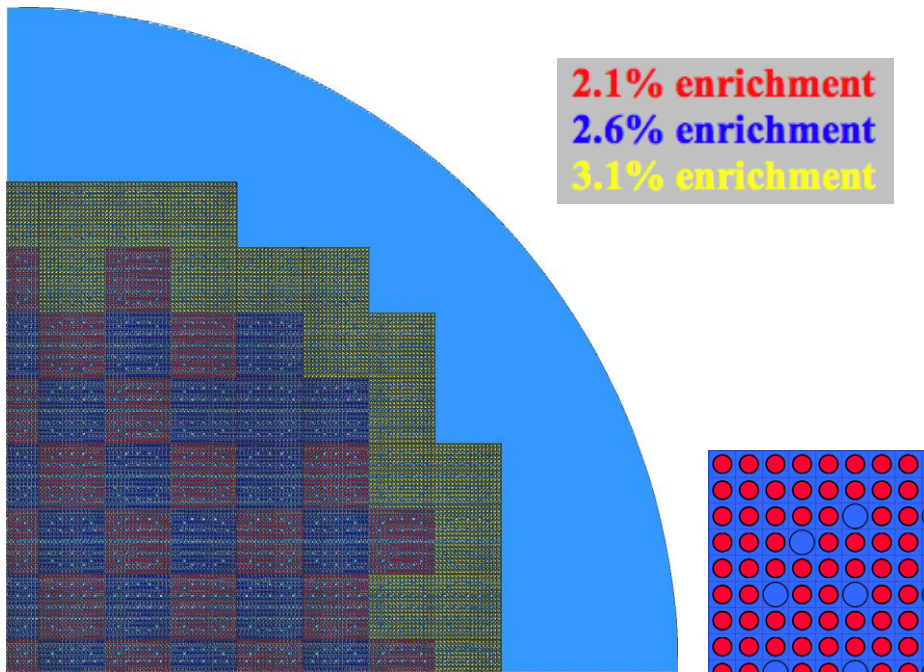


Fig. 2. Quadrant of whole-core, quarter-symmetric, PWR model, with section of 17x17 pin lattice shown.

Fig. 3 plots the fundamental eigenvector for four different meshes: 10x10x1, 15x15x1, 30x30x1, and 60x60x1. The batch sizes are 500 k, and fission matrix tallying is performed from cycle 4 to 55. The 15x15x1 mesh corresponds to assembly-size regions, the 30x30x1 mesh corresponds to quarter-assembly-size regions, and the 60x60x1 mesh corresponds to 1/16th-assembly-size regions. The 10x10x1 mesh does not match assembly geometry, and is shown as an example of a bad mesh choice. Fission outside of two assembly lengths are nonlocal, which results in about 0.5% of fissions being put into the local region. In the 60x60x1 case, sparsifying reduces the storage requirement from 99 MB to 8 MB.

Fig. 4 show the real part of the eigenvalue spectrum for the aforementioned meshes and a 5x5x1 and 120x120x1 mesh. The number of nonzero eigenvalues is equal to the rank of the fission matrix—the number of fissionable spatial regions. When the mesh is finer, we can see further out in the spectrum—the better the continuous spectrum is approximated. The imaginary component of the spectrum is initially at zero and takes on larger values further out, which we address below.

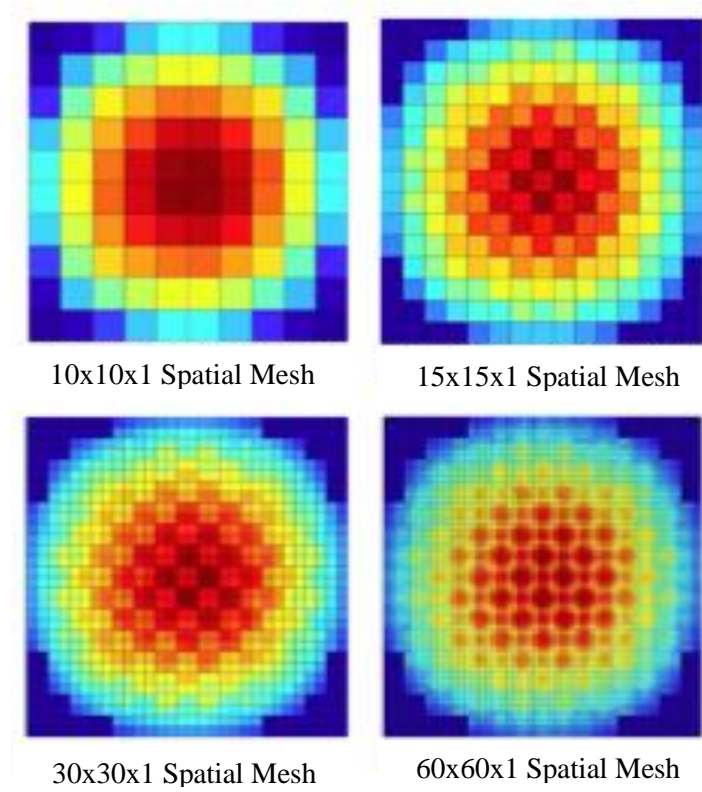


Fig. 3. 2D PWR fundamental eigenmodes for 4 spatial meshes. Fission matrix tallied for cycles 4-55, with a batch size of 500 k.

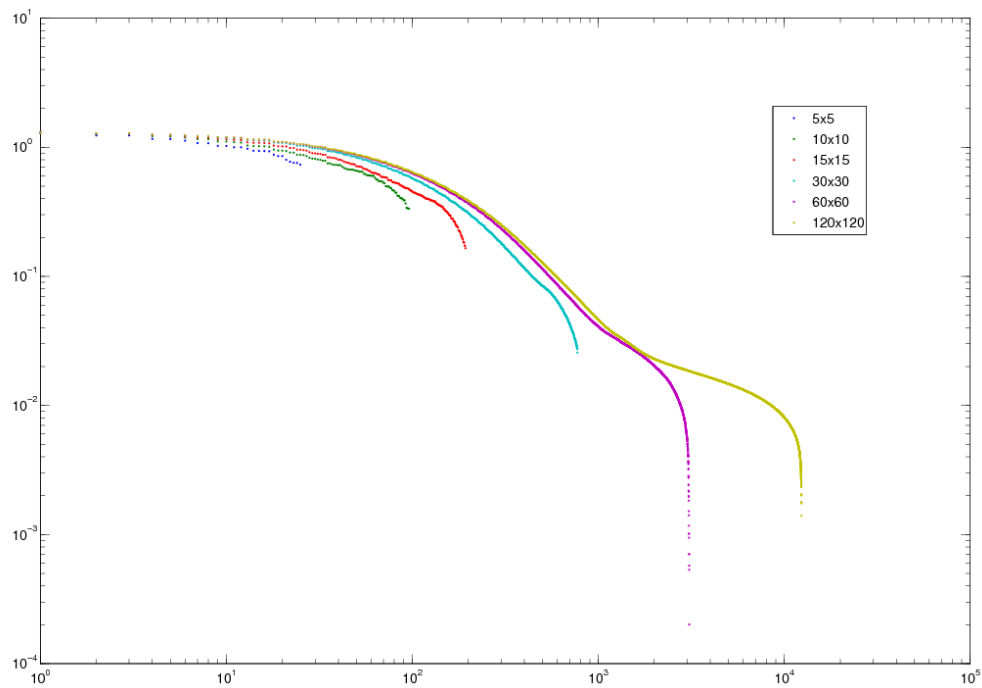


Fig. 4. Real component of eigenvalue spectrum for 2D PWR problem. Six different spatial resolutions are shown.

Fig. 5 examines the convergence behavior of the first 10 eigenvalues with increasingly fine meshing. The higher the eigenvalue, the more sensitive it is to the mesh size—the finer the required mesh. With this plot we see the meshing requirement on a realistic problem for accurate fission matrix answers, which for these quantities is around a 60x60x1 spatial mesh. Hence, this method hasn't been pursued in the past due to the significant storage needed.

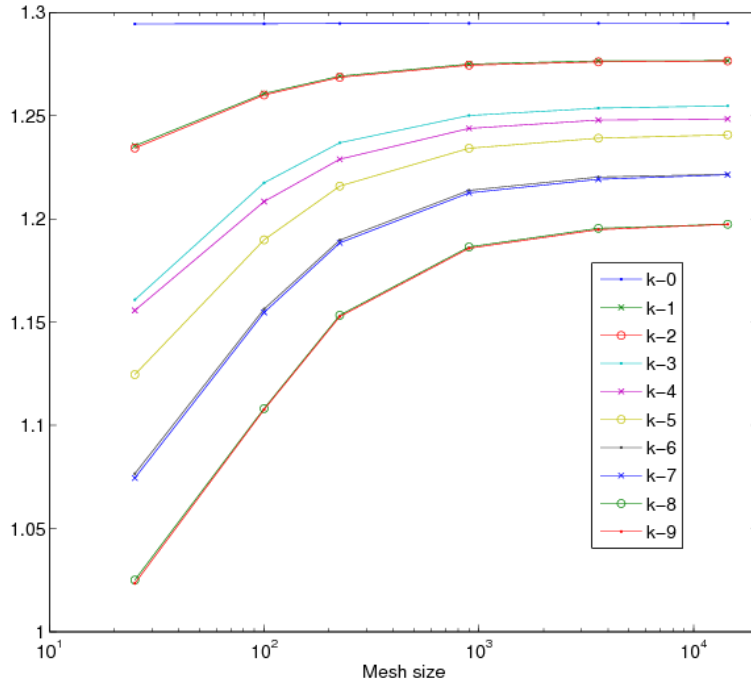
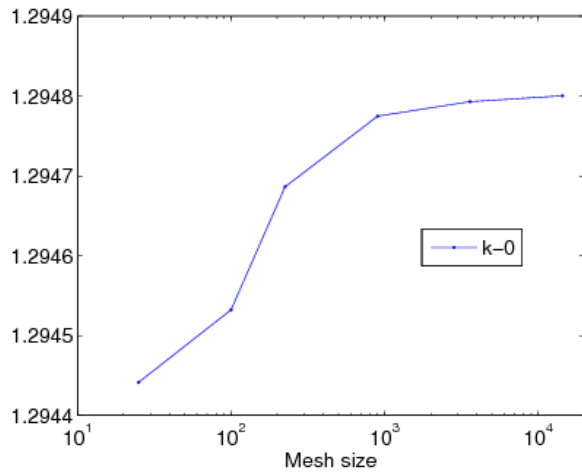


Fig. 5. Eigenvalue convergence behavior for increasingly fine meshing, 2D PWR problem.

Fig. 6 gives a closer view of the fundamental eigenvalue only.



# Mesh regions	K_0
5x5 = 25	1.29444
10x10 = 100	1.29453
15x15 = 225	1.29469
30x30 = 900	1.29477
60x60 = 3600	1.29479
120x120 = 14400	1.29480

Fig. 6. Fundamental eigenvalue convergence behavior for increasingly fine meshing, 2D PWR problem.

There is the question of the effect the sparse approximation has on the results. Fig. 7 plots the percentage difference in real parts of the eigenvalue spectra for the 30x30x1 spatial mesh case, where the full spectrum is the reference. The differences oscillate and grow, and only reach a maximum of 2.5%. This agrees with our observations that the higher the eigenmode, the more sensitive it is to noise. As to the reason for the oscillations, we are unsure. Since only a fraction of the spectrum, on the low end, is of concern due to spatial discretization, the plot confirms sparsifying does not significantly affect the eigenvalues of interest.

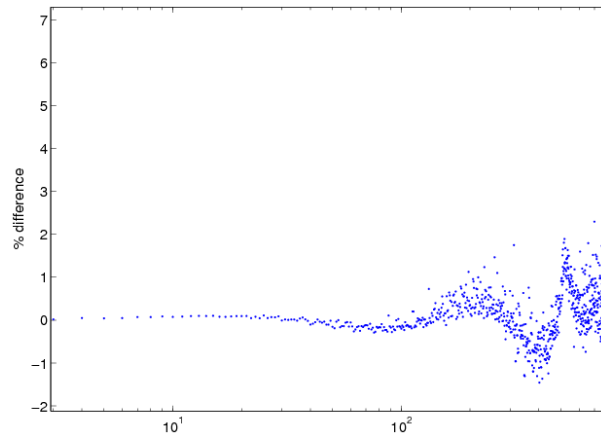


Fig. 7. Percentage difference in sparse and full eigenvalue spectra for the 30x30x1 spatial mesh, 2D PWR problem: $(k_{i,\text{sparse}} - k_{i,\text{full}}) / k_{i,\text{full}}$.

Fig. 8 shows the same type of percentage difference, but for the fundamental eigenvector. The difference is mostly zero, but on the bottom left there is an element that the sparse approximation overestimates by 30%. This occurs because the region is adjacent to non-fissionable material, water in this case. When moving nonlocal fission to the edge of the local region, the region chosen must be fissionable (checked by looking at the accumulated fission matrix denominator). If this check is not in place, the eigenvector gives a nonzero fission rate in a region with only water. This checking can have the effect, as seen here, of pushing too many nonlocal fissions into one region. To fix this, nonlocal weight may have to be smeared over multiple local regions. Fig. A.1 shows the sparse vs. full percentage difference for the first 16 eigenmodes.

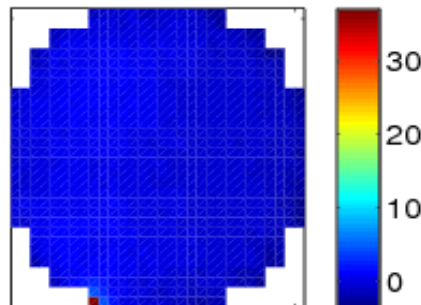


Fig. 8. Percentage difference in sparse and full fundamental eigenvectors for the 30x30x1 spatial mesh, 2D PWR problem: $(s_{i,\text{sparse}} - s_{i,\text{full}}) / s_{i,\text{full}}$.

Figs. 9 and 10 show the effect of reduced statistical uncertainty on the real and imaginary components of the eigenvalue spectra for the 120x120x1 spatial mesh case. The blue points are results from a matrix with twice as many samples. The real eigenvalue spectrum calculated from the better-sampled matrix can look further out before dropping to zero. Also, the imaginary components get smaller with increased precision—empirical evidence that the imaginary components of the spectrum result from noise.

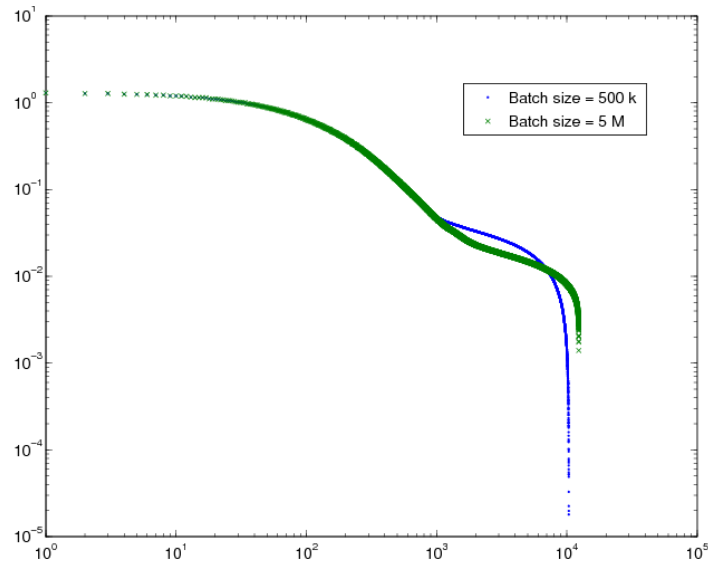


Fig. 9. Real component of eigenvalue spectra for two batch sizes for the 120x120x1 spatial mesh, 2D PWR problem. Fission matrix tallied for cycles 4-100.

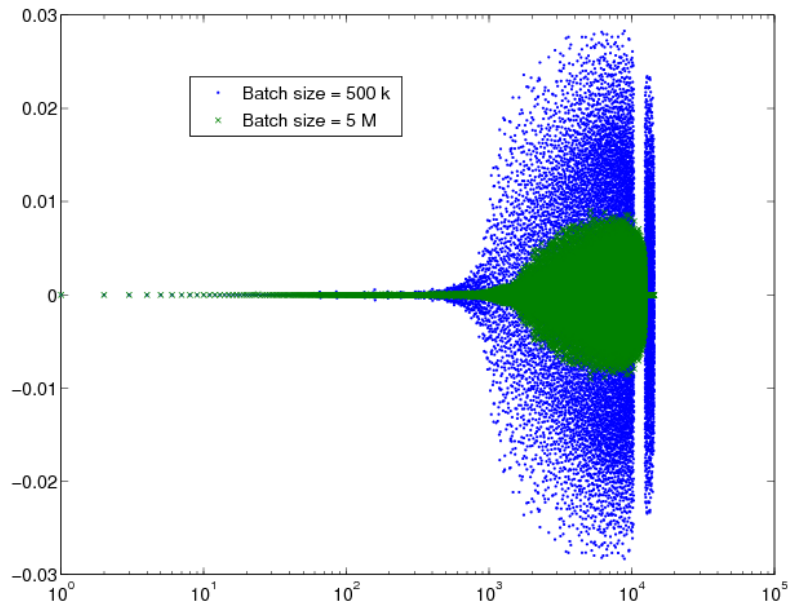


Fig. 10. Imaginary component of eigenvalue spectra for two batch sizes for the 120x120x1 spatial mesh, 2D PWR problem. Fission matrix tallied for cycles 4-100.

Fig. 11 shows the first 16 eigenmodes for the 120x120x1 spatial mesh. These shapes in general match with what is found in Ref. [5]. Table 1 shows the corresponding eigenvalues. There is evidence of multiplicity: similarly shaped eigenvectors have eigenvalues close together (#1,2 ; 6,7 ; 8,9 ; 13,14). The slight differences are due to noise, as the model's symmetry gives no reason to believe they shouldn't be the same.

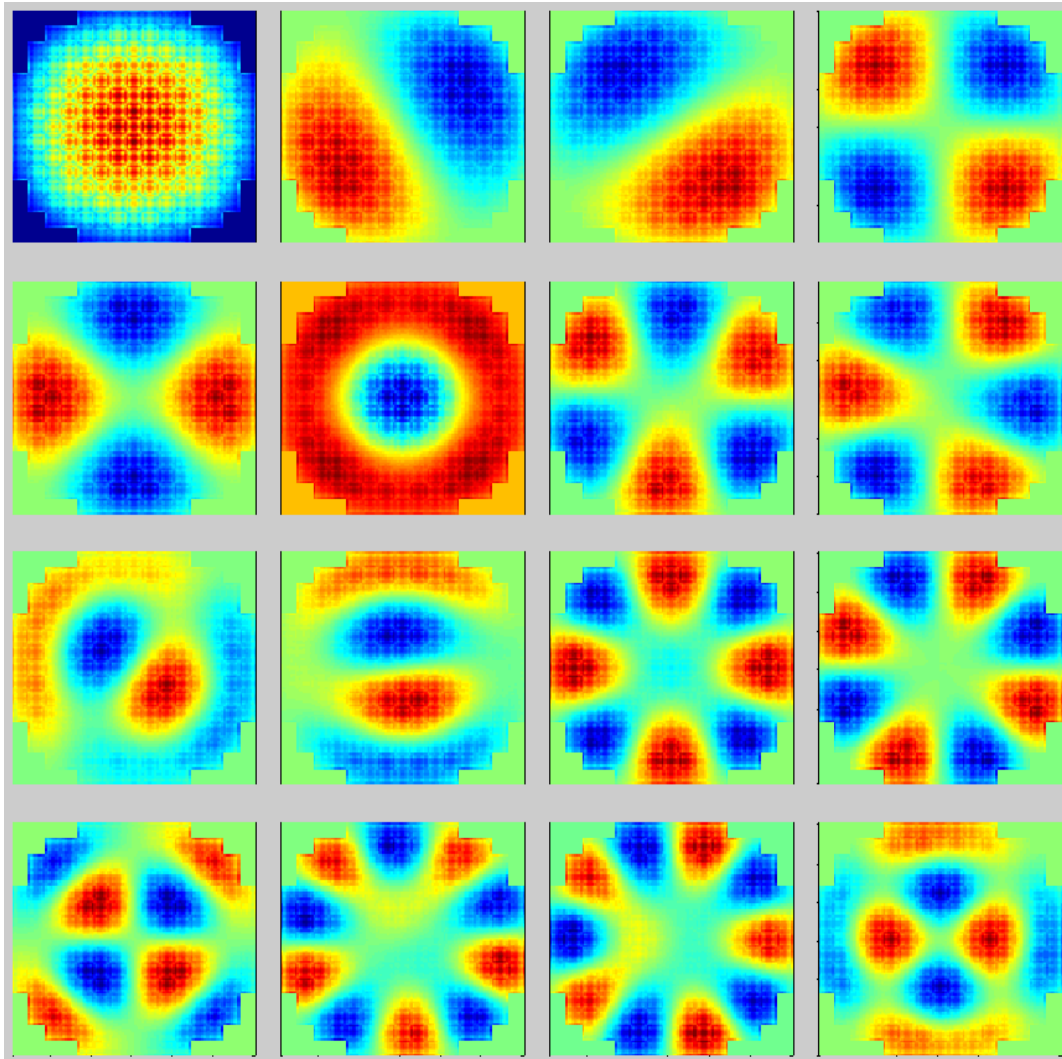


Fig. 11 First 16 eigenmodes for 120x120x1 mesh, 2D PWR problem. Fission matrix tallied for cycles 4-100, with a batch size of 5 M.

Table 1 First 16 eigenvalues for 120x120x1 spatial mesh, 2D PWR problem. Fission matrix tallied for cycles 4-100, with a batch size of 5 M.

n	k_n		n	k_n
0	1.29480		8	1.19745
1	1.27664		9	1.19743
2	1.27657		10	1.18825
3	1.25476		11	1.18305
4	1.24847		12	1.15619
5	1.24075		13	1.14633
6	1.22160		14	1.14617
7	1.22141		15	1.14584

Figs. A.2 and A.3 show the first 100 eigenmodes for batch sizes of 500 k and 5 M. From the differences between the two plots we can examine the sensitivity of different eigenmodes to fission matrix noise. Note there are some sign changes between the two plots, due to the MATLAB solver. We can see that the radially symmetric modes differ least between the two batch sizes, indicating they are the quickest to converge. Modes that aren't radially symmetric, including modes #1 and #2, appear to be quite sensitive to statistical uncertainty in the fission matrix.

Much of transport theory relies on the assumption that functions can be expanded in terms of the eigenfunctions of the fission kernel. This is equivalent to assuming a self-adjoint, or symmetric, fission matrix, which corresponds to orthogonal eigenmodes. This assumption is only rigorously true for problems with no energy dependence. With the fission matrix, we can examine the validity of the assumption for continuous energy problems. Fig. 12 plots the magnitude of the inner products of the first 25 eigenmodes for the 120x120x1 spatial mesh. The diagonal is unity due to normalization. Most inner products off the diagonal are close to zero, which gives credence to the orthogonality assumption for this problem. The largest off-diagonal values correspond to inner products of adjacent modes with similar shapes. All eigenmode pairs with multiplicity listed above have inner products of noticeable magnitude.

Homogenous 2D Reactor

When reflecting surfaces are added to a problem, it is well known that higher eigenmodes of the full problem are eliminated. This accelerates convergence in the Monte Carlo power iteration. With the fission matrix, we can directly observe this. Fig. 13 shows the higher eigenmodes for a homogenous 2D problem, with 0, 1, or 2 reflecting surfaces present in the geometry model. The corresponding spatial meshes are: 30x30x1, 15x30x1, and 15x15x1. The fission matrices are tallied for 51 cycles, and the batch sizes are 500 k. The higher eigenmodes of the half-core model correspond to the eigenmodes symmetric about the y-axis in the whole core model. Similarly, the higher eigenmodes of the quarter-core model correspond to the quarter symmetric eigenmodes of the whole core model. Figs. A.4, A.5, and A.6 show the first 16 eigenmodes for all 3 models.

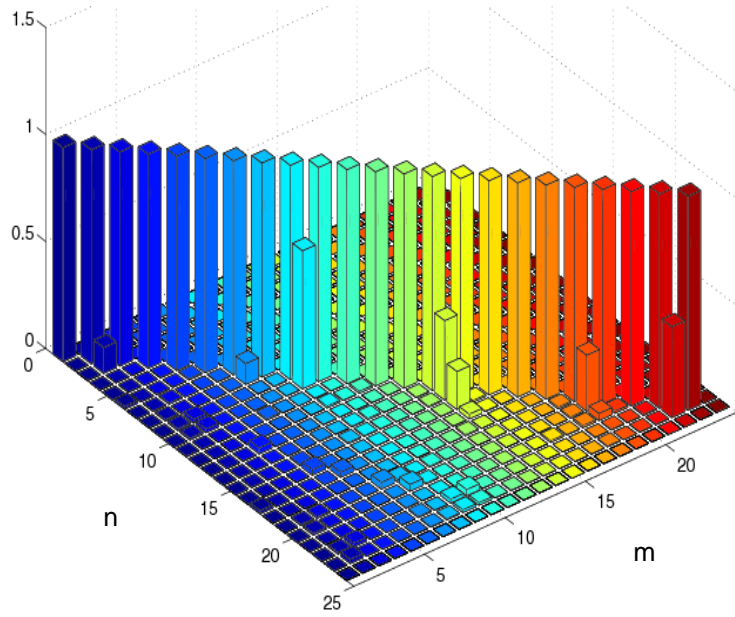


Fig. 12. Magnitude of inner products ($\#n$ and $\#m$) of first 25 forward eigenfunctions for 2D PWR problem, 120x120x1 spatial mesh. Fission matrix tallied for cycles 4-100, 5 M batch size.

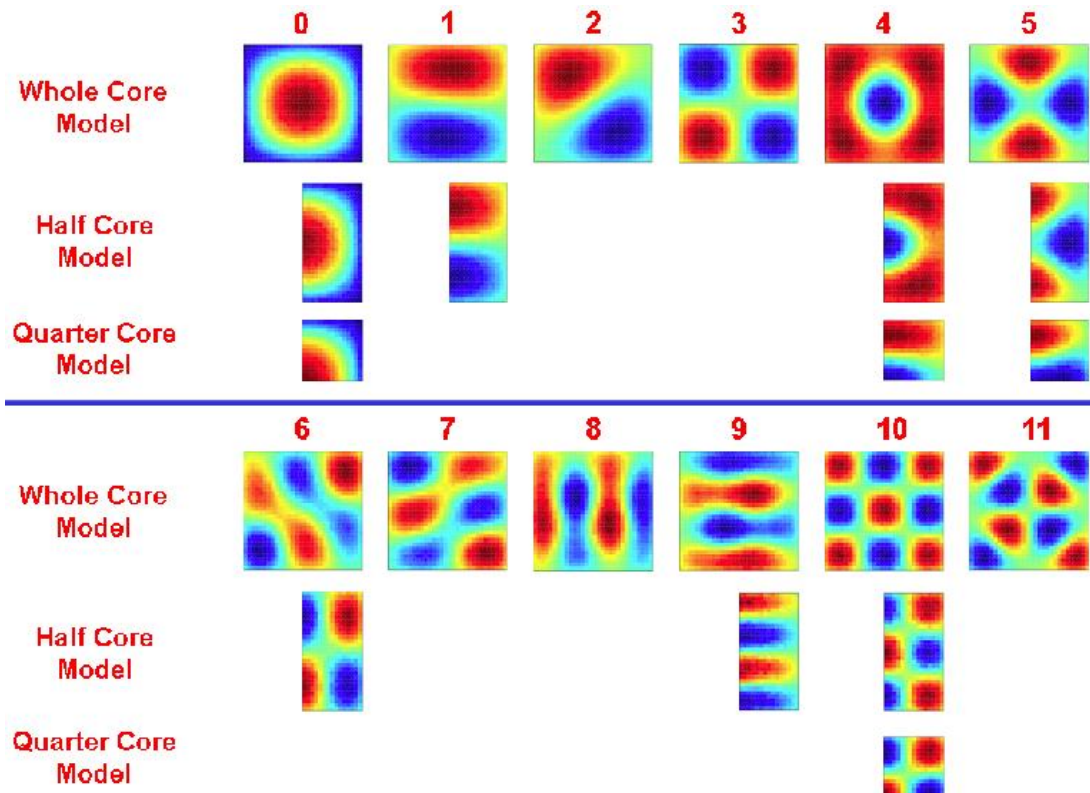


Fig. 13. Higher eigenmodes for whole-core (30x30x1 spatial mesh), half-core (15x30x1 spatial mesh), and quarter-core (15x15x1 spatial mesh) models of 2D homogenous reactor. Fission matrices tallied for cycles 4-55, with batch size of 500 k.

Kord Smith Challenge

The Kord Smith Challenge problem [7] is a detailed 3D PWR model. Starting with a flat guess, Monte Carlo source convergence takes about 50 cycles. Fig. 14 shows this convergence behavior along with the fission matrix behavior. The spatial mesh is $42 \times 42 \times 20$, corresponding to quarter assembly meshes in the xy plane. The fission matrix was tallied for cycles 4-55, with a batch size of 1M. Fig. 14 plots the: fundamental eigenvalue, the dominance ratio estimate from fission matrix power iteration, and the Shannon entropy for the unaffected Monte Carlo fission bank and the fission matrix eigenvector. While the Monte Carlo fission source takes about 50 cycles to converge, the fission matrix fundamental eigenpair converges instantly. The first data points are from a fission matrix with 3M samples.

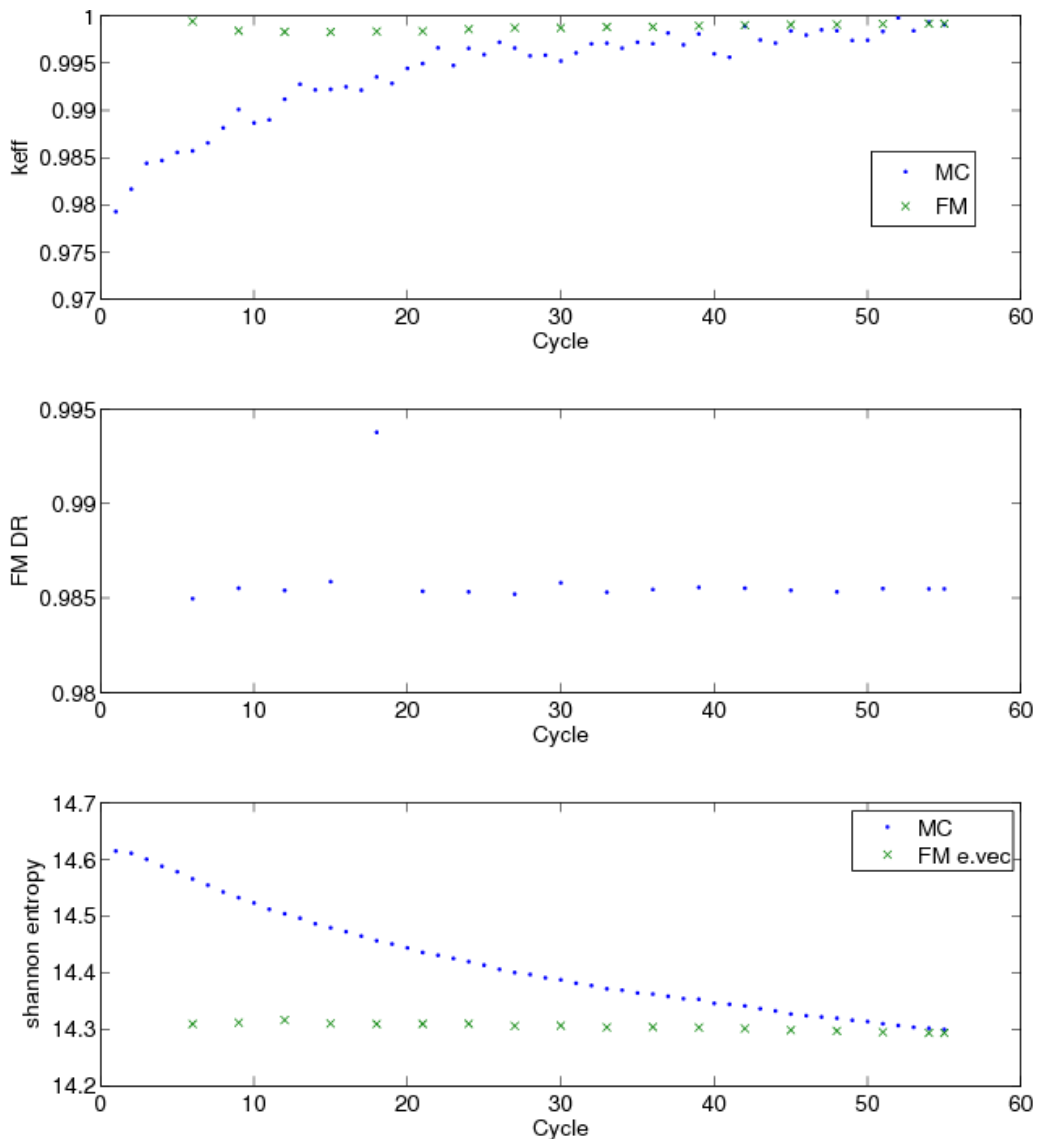


Fig. 14. Fundamental eigenvalue, dominance ratio estimate from fission matrix power iteration, and Shannon entropy convergence behavior for unaffected Monte Carlo fission bank and fission matrix eigenvector. Kord Smith Challenge, $42 \times 42 \times 20$ spatial mesh. Fission matrix tallied for cycles 4-55, batch size of 1 M.

Fig. 15 shows the same plot, but for the 21x21x20 spatial mesh case, and now for 200 cycles instead of 55. Again we see quick convergence, but not as quickly as the finer mesh case. There is a noticeable positive bias in the Shannon entropy of the fission matrix eigenvector for the coarser mesh, due most likely to the discretization error. This positive bias persists at cycle 200.

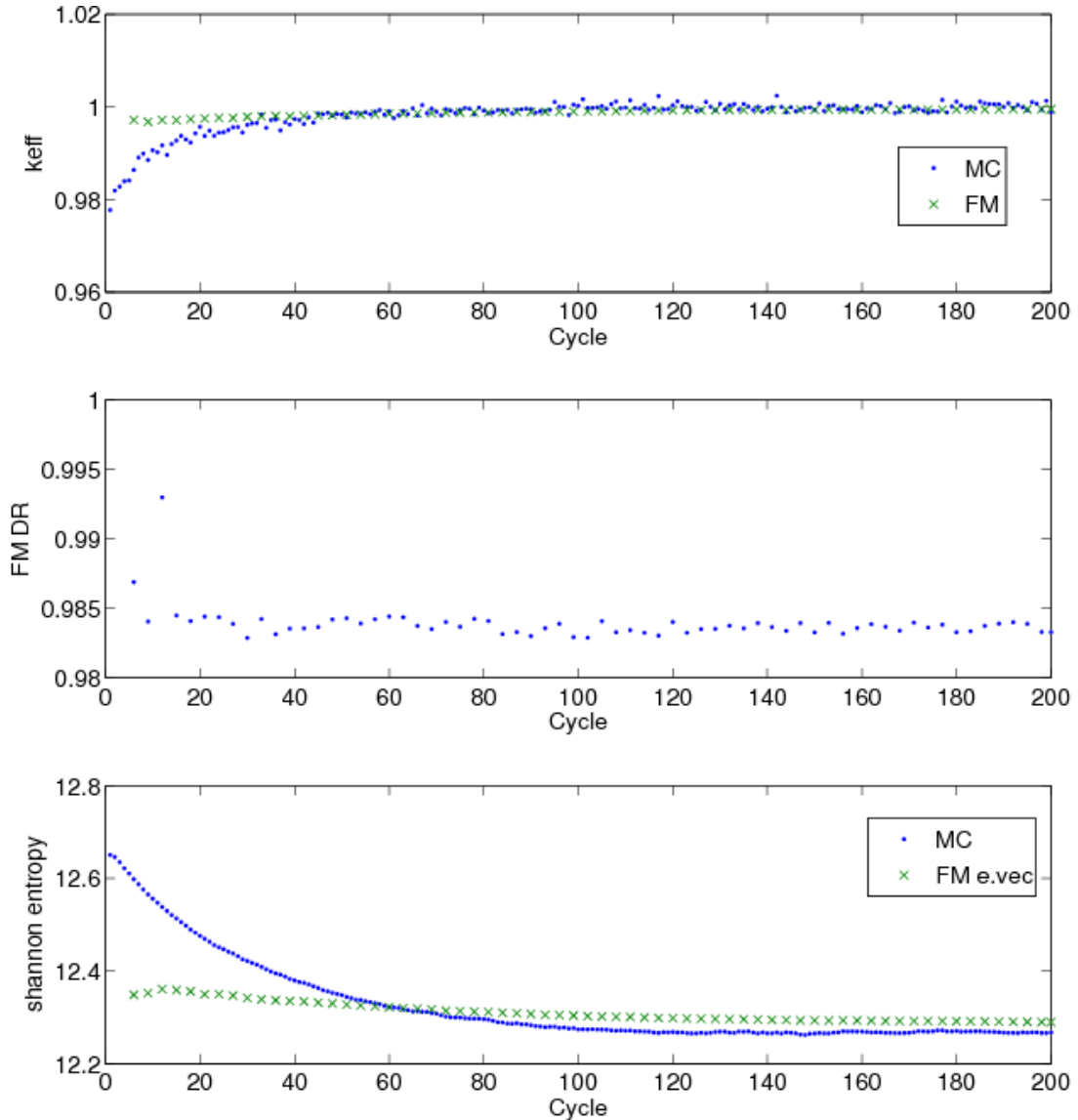


Fig. 15. Fundamental eigenvalue, dominance ratio estimate from fission matrix power iteration, and Shannon entropy convergence behavior for unaffected Monte Carlo fission bank and fission matrix eigenvector. Kord Smith Challenge, 21x21x20 spatial mesh. Fission matrix tallied for cycles 4-200, batch size of 1 M.

Figs. 16 and 17 show the eigenvalue spectrum of this problem. As before, a finer mesh raises the real part of the eigenvalue spectrum. Table 2 gives the first 15 eigenvalues for the 42x42x20 spatial mesh.

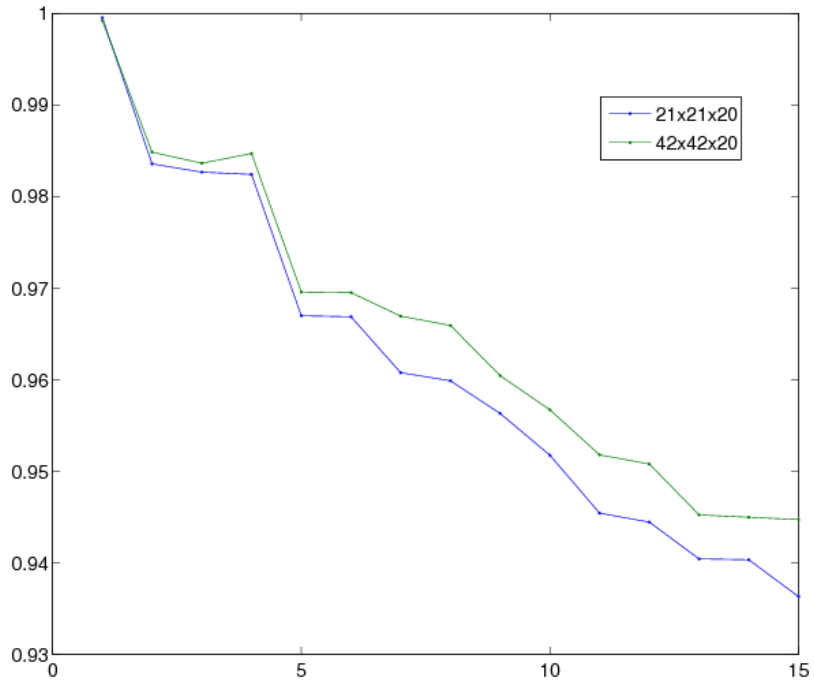


Fig. 16. First 15 eigenvalues (no imaginary components) of the Kord Smith Challenge, for two spatial mesh sizes: 21x21x20 and 42x42x20.

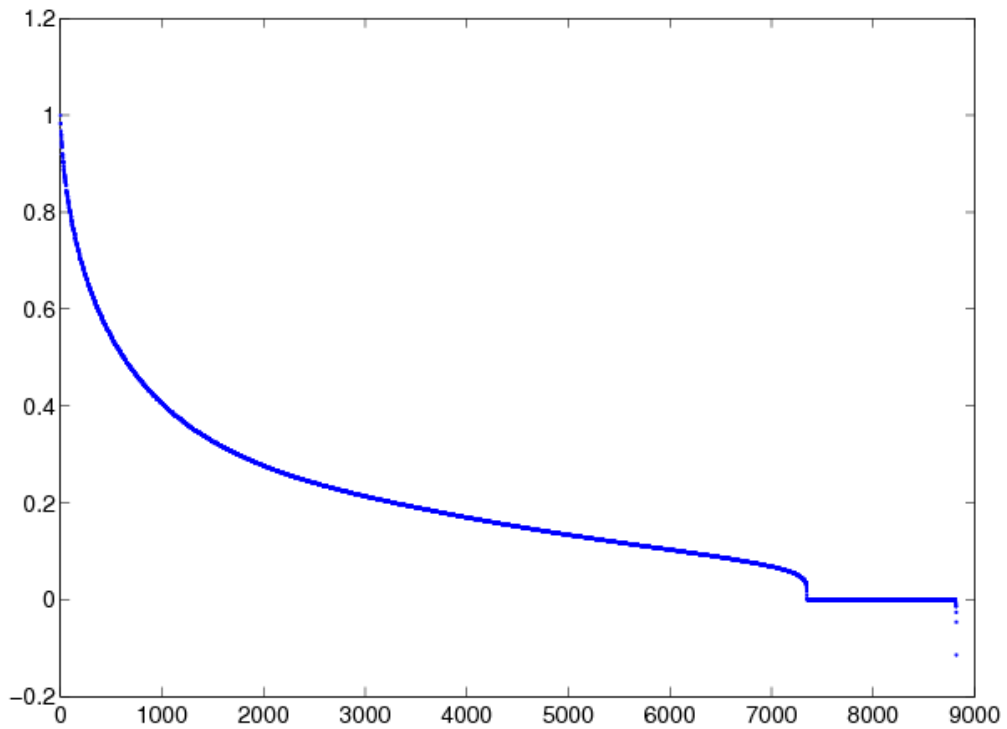


Fig. 17. Entire real part of the eigenvalue spectrum of the Kord Smith Challenge for the 21x21x20 spatial mesh.

Table 2 First 15 eigenvalues for the Kord Smith Challenge, with a 120x120x1 spatial mesh.

n	k_n	n	k_n
0	0.99919	8	0.96043
1	0.98483	9	0.95671
2	0.98362	10	0.95178
3	0.98469	11	0.95078
4	0.96956	12	0.94524
5	0.96950	13	0.94497
6	0.96693	14	0.94472
7	0.96591	-	-

Figs. 18 and 19 show the first 15 eigenmodes for the Kord Smith Challenge. Most shapes are familiar from the 2D PWR problem, but extra modes are now present due to the axial dependence. As in the 2D PWR problem, we see eigenmode multiplicity due to the x-y quarter symmetry (#1,3 ; 4,5 ; 13,14). The y-z plane eigenmodes reveal the axial asymmetry. In addition to the fundamental mode being bottom peaked, we also see other modes with greater magnitudes at the bottom of the core. This is due to the cold moderator in the bottom half.

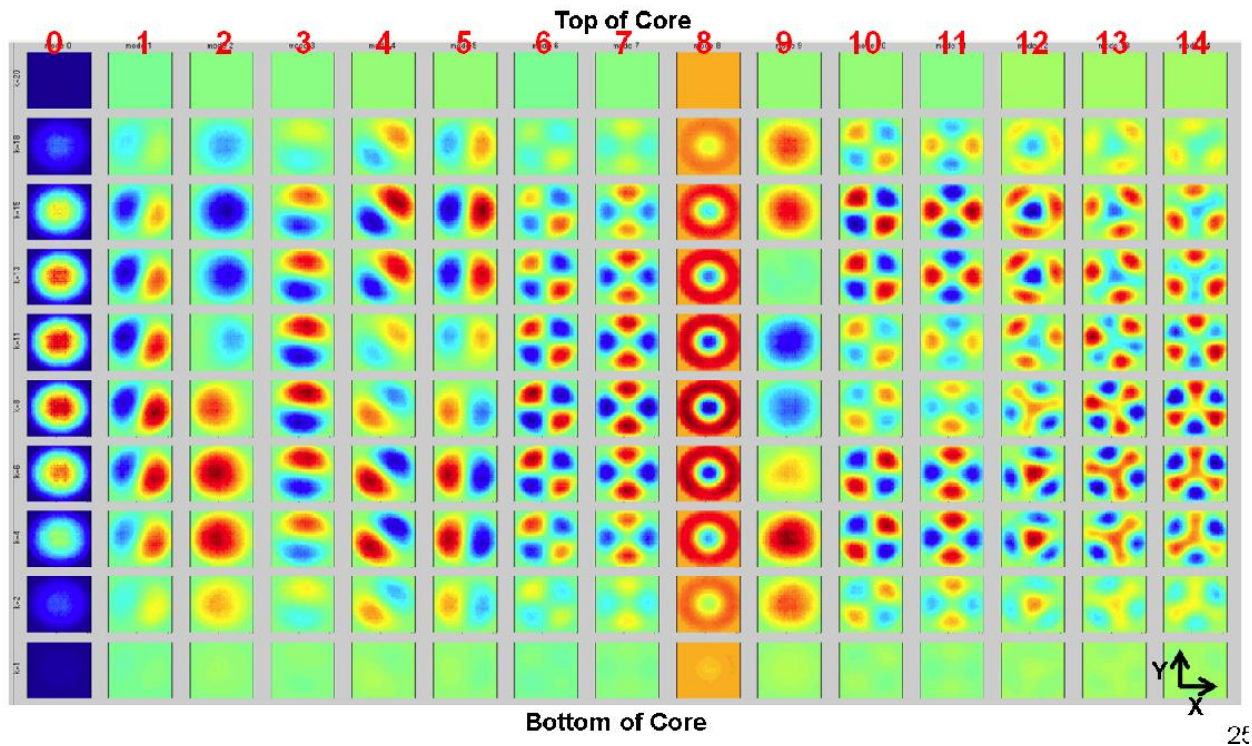


Fig. 18. First 15 eigenmodes for Kord Smith Challenge, 42x42x20 spatial mesh. Ten XY planes are shown. Fission matrix tallied for cycles 4-200, batch size of 1 M.

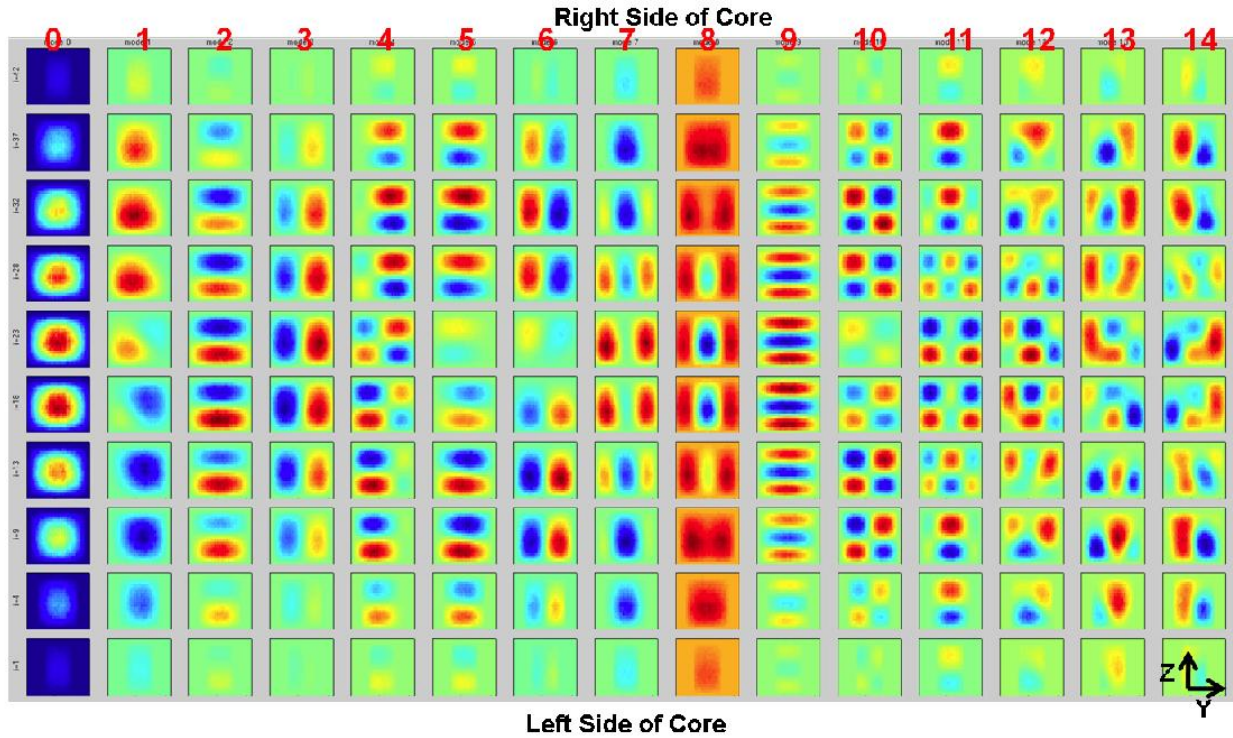


Fig. 19. First 15 eigenmodes for Kord Smith Challenge, 42x42x20 spatial mesh. Ten YZ planes are shown. Fission matrix tallied for cycles 4-200, batch size of 1 M.

Fig. 20 shows the near-orthogonality of the eigenfunctions. Again, the highest off-diagonal inner products are those of eigenmodes with similar shapes. All eigenmode couples with multiplicity have high inner products.

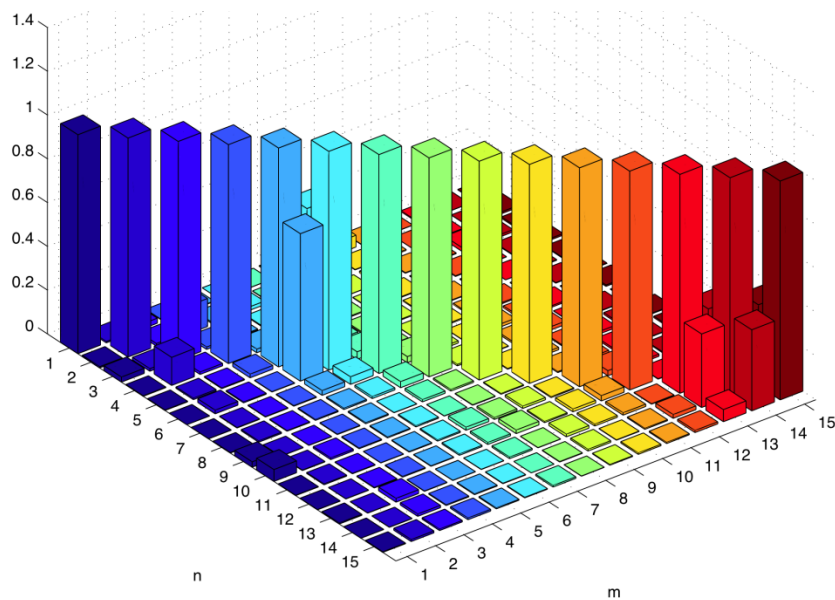


Fig. 20. Magnitude of inner products (n and m) of first 15 forward eigenfunctions for Kord Smith challenge, 42x42x20 spatial mesh. Fission matrix tallied for cycles 4-200, 1 M batch size.

Fig. C.1 shows a plot similar to Fig. 18, but with Silver-Indium-Cadmium control rods [17] fully inserted into one assembly. Fig. C.2 shows the depression of the first 15 eigenvalues due to the insertion.

Fuel Storage Vault Problem

The third realistic problem analyzed is Benchmark Problem 1 from the OECD/NEA Source Convergence Benchmarks [8]. This problem contains 36 large, loosely coupled spent fuel assemblies in water surrounded by concrete reflector. A sole assembly has concrete reflector on two sides, as opposed to one or zero for the others. Consequently, this single assembly is by far the most reactive, with a total fission rate over a factor of 10,000 greater than the least reactive assembly. Conventional Monte Carlo requires around 2000 cycles for fission source convergence with a flat initial guess.

Fig. 21 shows the convergence behavior of the unaffected Monte Carlo and fission matrix results. The fission matrix is tallied cycles 3-200, with a batch size of 1 M. The spatial mesh is 96x12x10, corresponding in the x-y plane to sixteen mesh regions for every assembly. By cycle 30, the fission matrix gives a reasonably converged fundamental eigenvector. Thus we see the potential for excellent source convergence acceleration with the fission matrix.

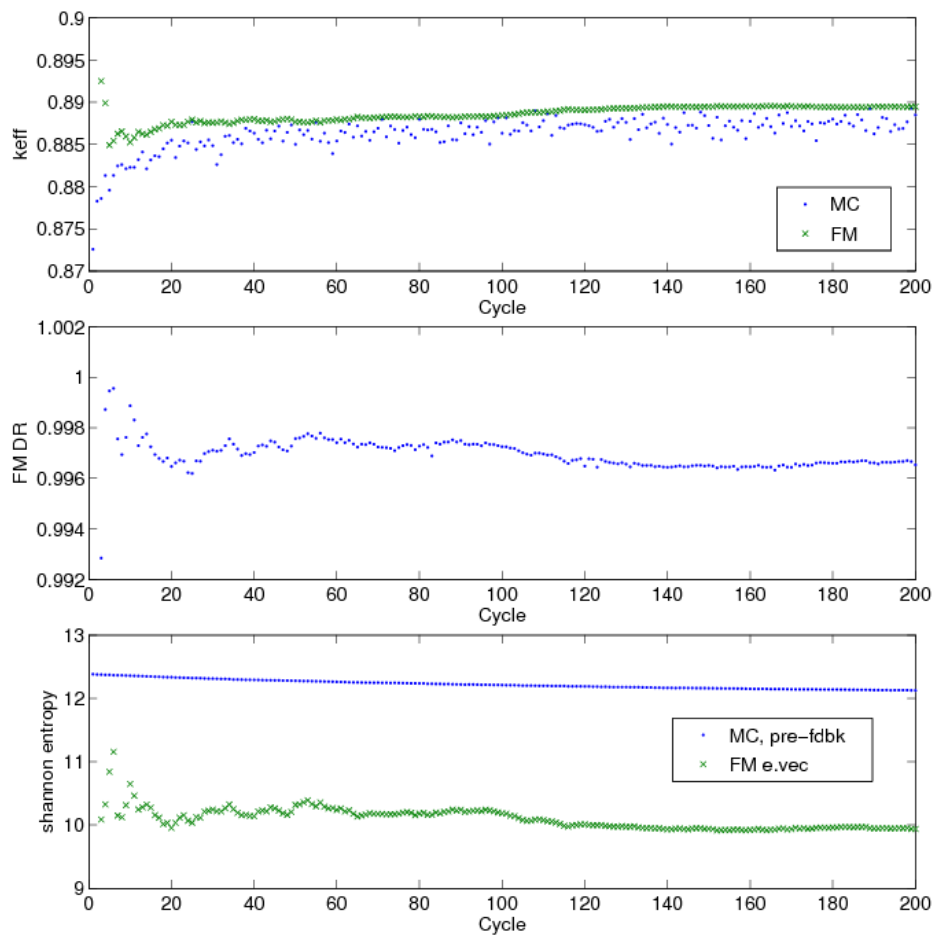


Fig. 21. Convergence behavior for the fuel storage vault problem, with a 96x12x10 spatial mesh. Fission matrix tallied cycles 3-200, batch size of 1 M.

Fig. 22 shows the first 16 eigenmodes of the fuel vault problem. The fundamental mode is largest in the top left assembly. We see increasing oscillations in the x-direction for higher eigenmodes.

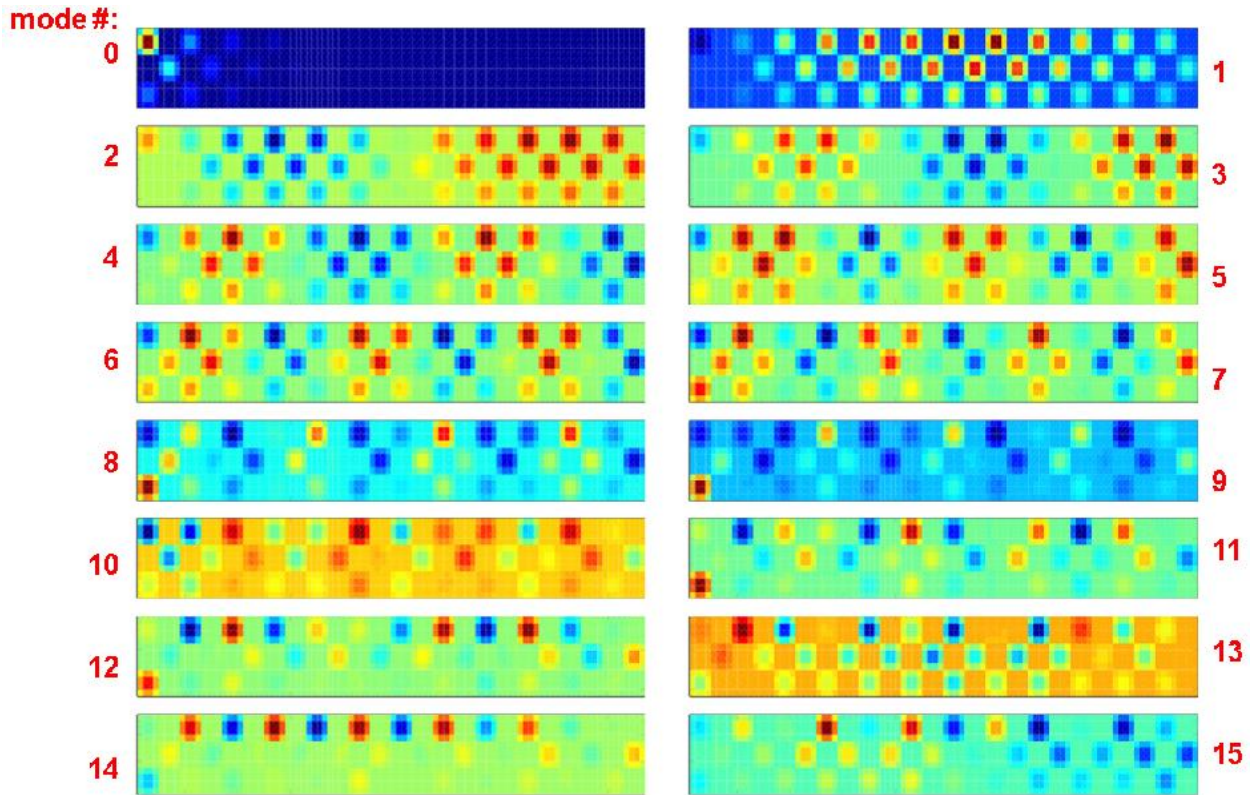


Fig. 22. First 16 eigenmodes of the fuel storage vault problem, with a 96x12x10 spatial mesh. Fission matrix tallied cycles 4-200, batch size of 1 M.

Fig. 23 shows the magnitudes of the inner products of the first 16 eigenfunctions. We see even greater orthogonality in this case, compared to the PWR problems. Fig. B.1 in the appendix gives the magnitudes of the inner products of the first 385 eigenfunctions. Most noticeable there is the apparent non-orthogonality for inner products with certain differences between index number. We do not have an explanation for this trend.

Fig. 24 plots the eigenvalue spectrum. It is noticeably more discontinuous than in the PWR problems. Since half of the mesh regions contain fissionable material, half of the spectrum is nonzero. Fig. 25 plots only the first 360 eigenvalues, from which we can gain some insight. The eigenvalues are noticeably grouped together—each group contains 36 values, and there are 10 total groups. This corresponds to the 36 loosely coupled fuel assemblies, and the are 10 axial meshes. Table 3 gives the first 16 eigenvalues.

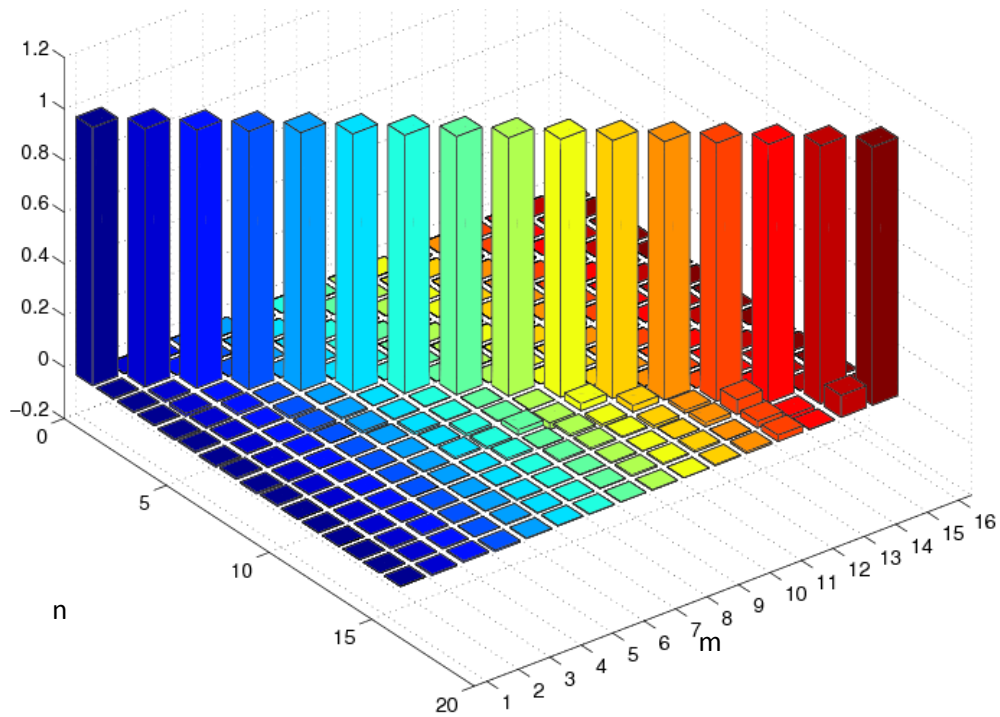


Fig. 23. Magnitude of inner products ($\#n$ and $\#m$) of first 16 forward eigenfunctions for fuel storage vault problem, 96x12x10 spatial mesh. Fission matrix tallied for cycles 3-200, 1 M batch size.

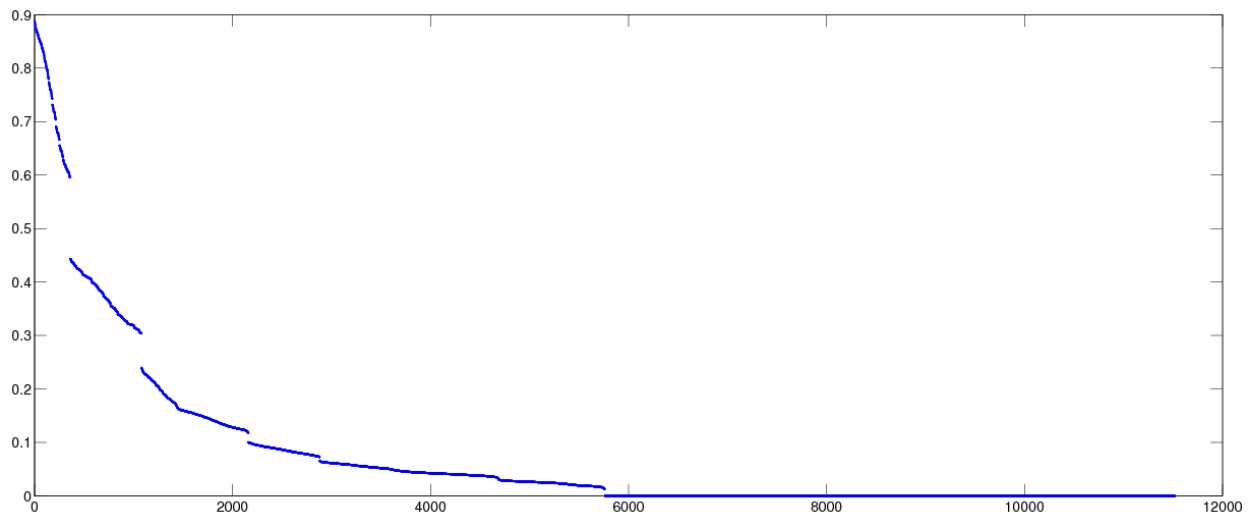


Fig. 24. Real part of the entire eigenvalue spectrum for the fuel storage vault problem, with 96x12x10 spatial mesh.

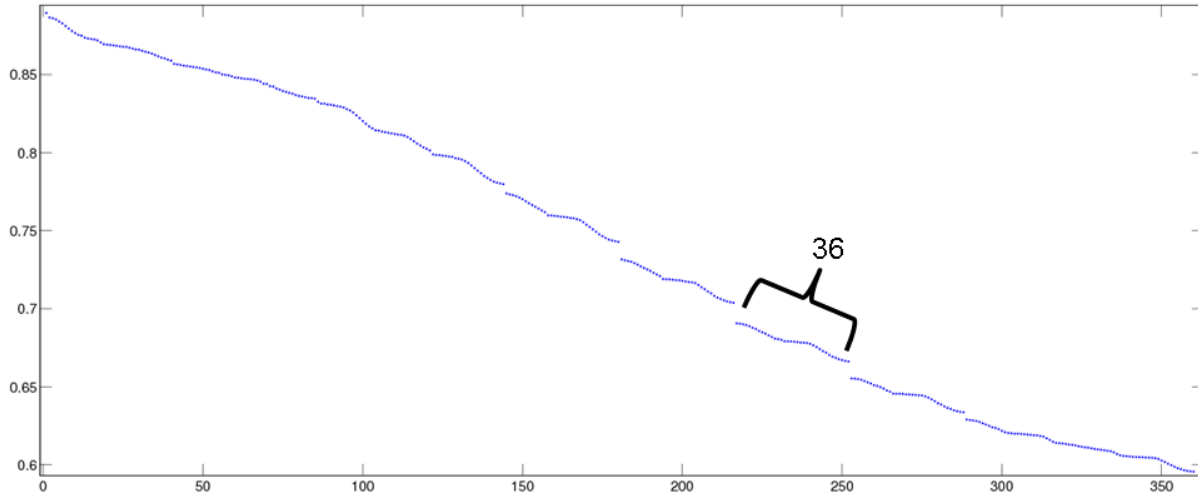


Fig. 25. Real part of the first 360 eigenvalues for the fuel storage vault problem, with 96x12x10 spatial mesh.

Table 3 First 16 eigenvalues for the fuel storage vault problem with a 96x12x10 spatial mesh.

n	k_n		n	k_n
0	0.88947		8	0.87785
1	0.88653		9	0.87658
2	0.88600		10	0.87536
3	0.88533		11	0.87488
4	0.88399		12	0.87363
5	0.88275		13	0.87309
6	0.88112		14	0.87279
7	0.87945		15	0.87245

Advanced Test Reactor

The final realistic problem examined is the Advance Test Reactor (ATR) at Idaho National Laboratory [9]. Used primarily for the study of radiation effects, this core has a complex serpentine-shape fuel arrangement which does not easily adhere to a Cartesian mesh. There are 40 curved fuel assemblies with 93% enriched uranium aluminide powder fuel; each wraps 45 degrees. Each assembly has 19 plates of thickness 0.2 cm; the actual thickness of the fuel within each plate is 0.05 cm.

Fig. 26 plots four different fission matrix columns onto the geometry of the ATR, without a sparse approximation for a 100x100x1 spatial mesh. The origin region of each plot is at or near the peak value. The values give the number of fission neutrons produced from the average neutron born in the origin region. We see that the problem is highly coupled—the average birth-to-fission distance is near the size of the actual problem. Thus a sparse approximation will not be useful here. Fig. 27, the fission matrix structure for a 50x50x1 spatial mesh, clearly illustrates this. Also, this problem suggests the benefit of

only allocating memory for fissionable regions; the rank of the allocated fission matrix is around half of its size.

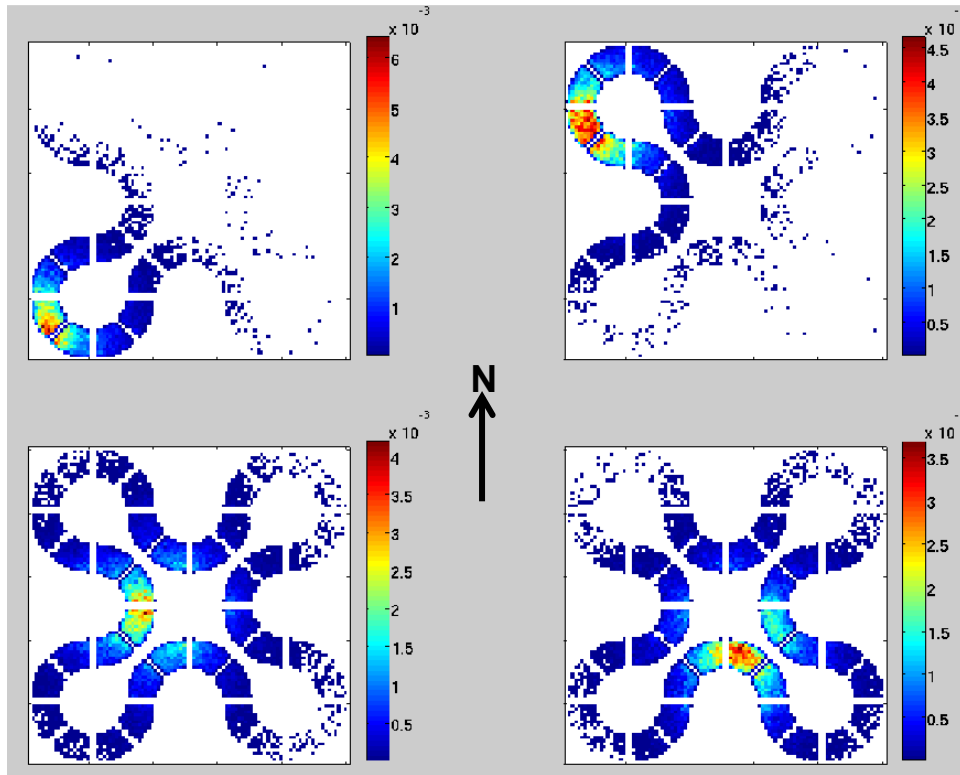


Fig. 26. Four full fission matrix columns for the ATR, 100x100x1 spatial mesh. Fission matrix tallied for cycles 2-200, batch size of 1 M.

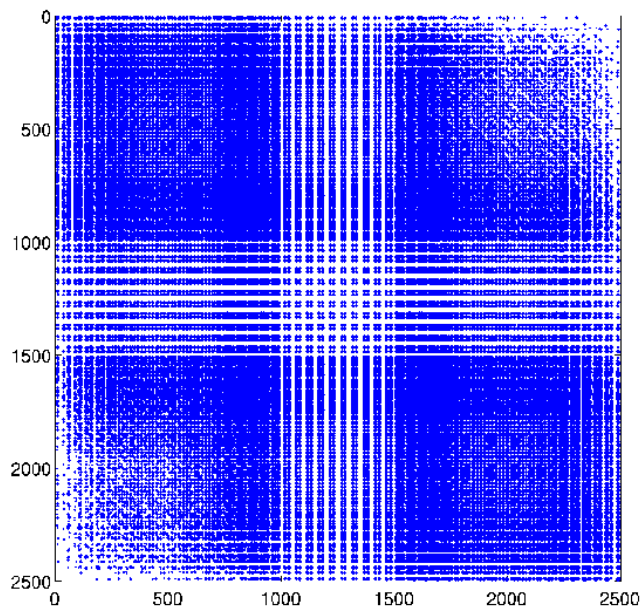


Fig. 27. Fission matrix structure for 50x50x1 spatial mesh, ATR problem. Fission matrix tallied for cycles 2-100, batch size of 500 k.

Fig. 28 shows the convergence behavior for this problem. Monte Carlo converges quickly, as this is a small problem with a low dominance ratio. The Shannon entropy plot shows a noticeable positive bias in the fission matrix fundamental eigenvector. The mesh width here 0.76 cm, whereas the fuel thickness of a single plate is only 0.05 cm. This large size difference suggests that the bias is due to discretization error—the mesh is much coarser than the scale of the model’s material variation.

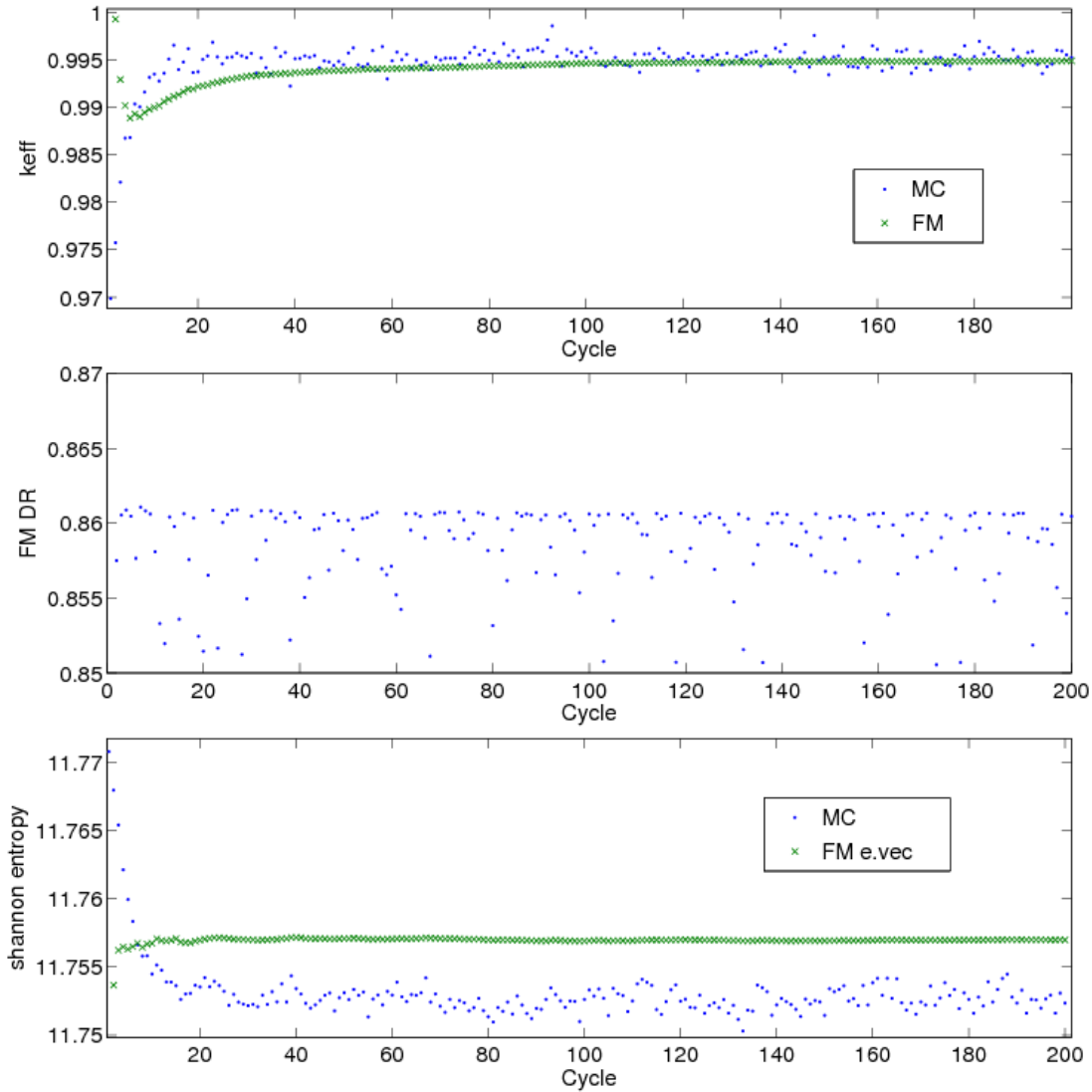


Fig. 28. Convergence behavior for the ATR problem, 100x100x1 spatial mesh. Fission matrix tallied for cycles 2-200, batch size of 1 M.

Fig. 29 shows the fundamental eigenvector for the ATR problem, and Fig. 30 shows the first 16 eigenvectors. Eigenmodes #0-3 are recognizable from the PWR results, but for higher eigenmodes we see new shapes.

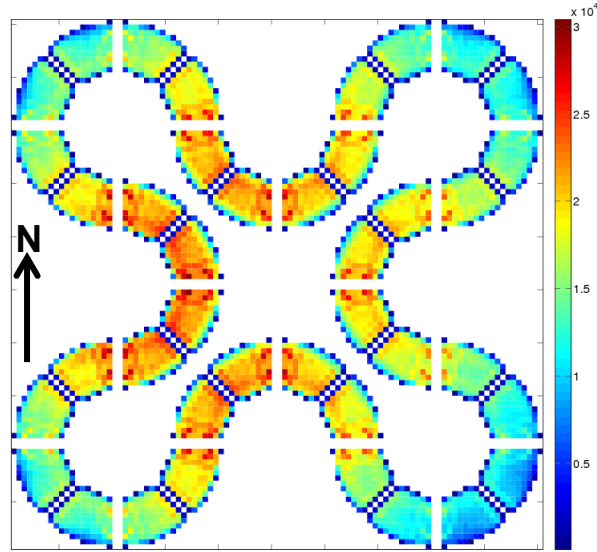


Fig. 29. Fundamental eigenvector of the fission matrix with $100 \times 100 \times 1$ spatial mesh, ATR problem. Fission matrix tallied for cycles 2-200, batch size of 1M.

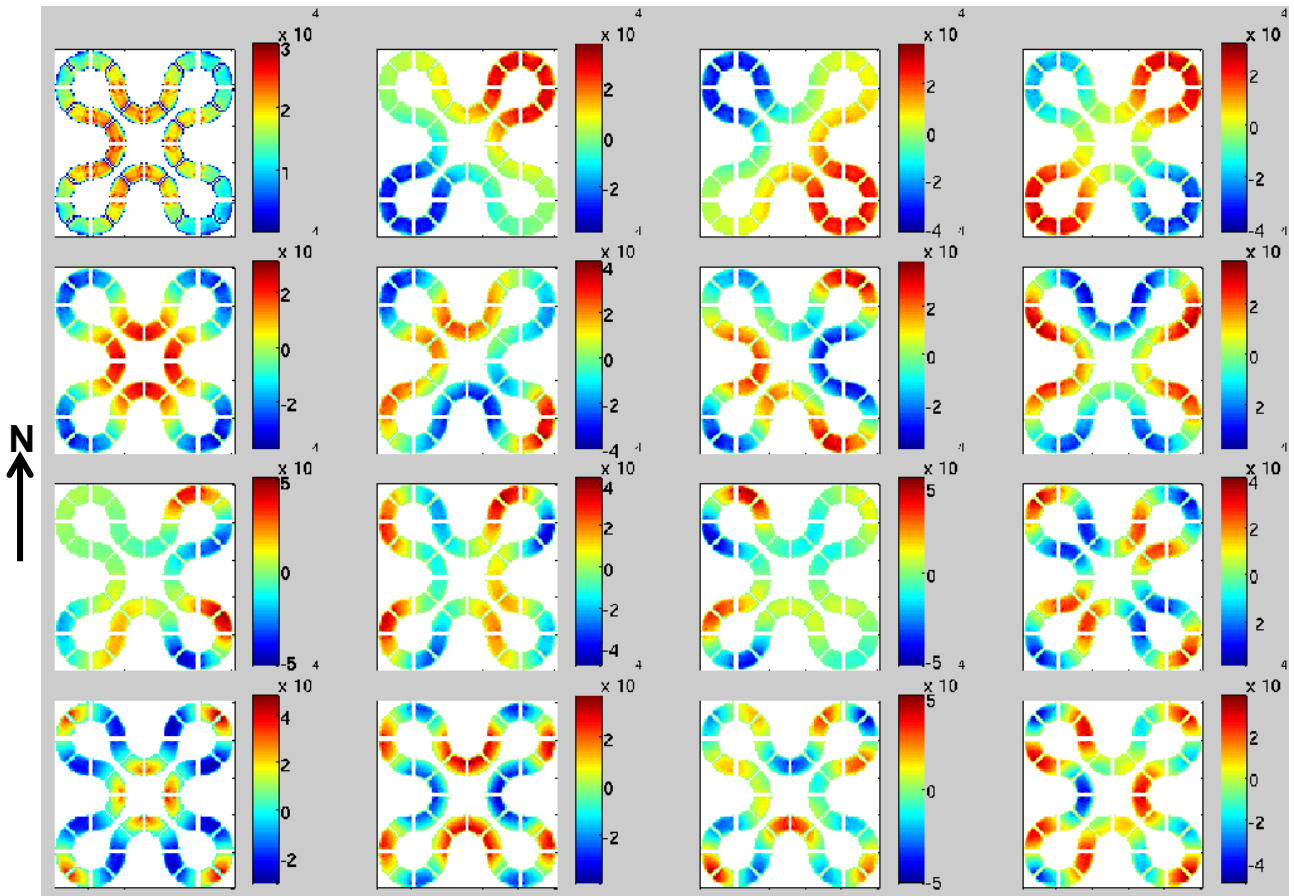


Fig. 30. First 16 eigenvectors of the ATR problem, with a $100 \times 100 \times 1$ spatial mesh. Fission matrix tallied for cycles 2-200, batch size of 1M.

Fig. 31 shows the eigenvalue spectrum for a 50x50x1 spatial mesh and 100x100x1 spatial mesh. The 50x50x1 spatial mesh results were found from a batch size of 500 k; the fission matrix was tallied for cycles 2-100. Table 4 gives the first 16 eigenvalues. As this is a small problem, we see a sharp decline in the eigenvalues.

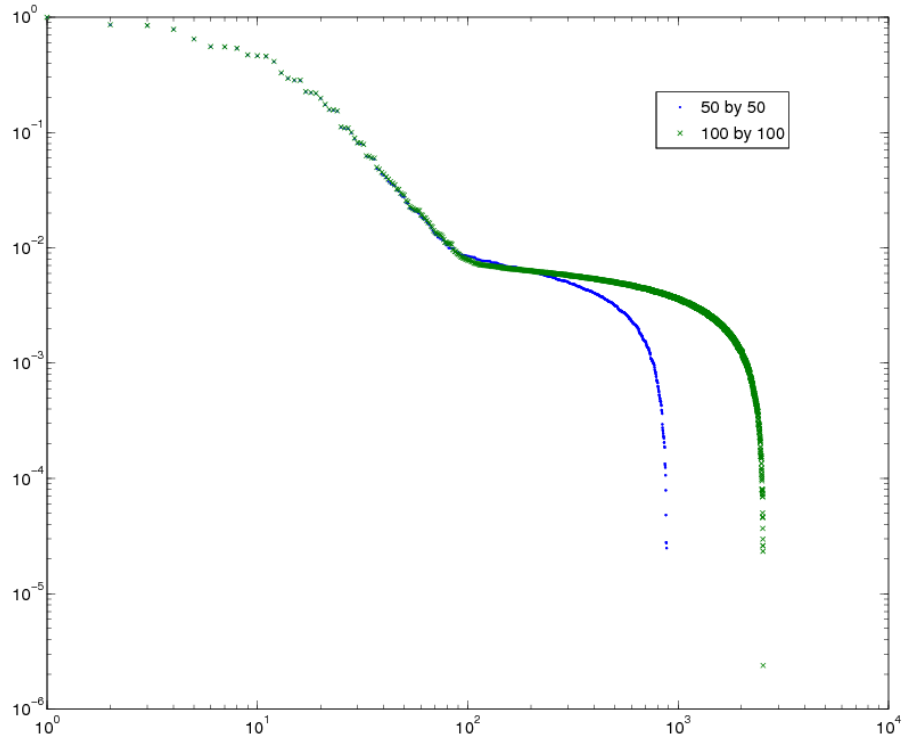


Fig. 31. Eigenvalue spectrums of the ATR problem, with a 100x100x1 spatial mesh.

Table 4 First 16 eigenvalues for the ATR, with a 100x100x1 mesh.

n	k_n		n	k_n
0	0.99490		8	0.47004
1	0.85630		9	0.46173
2	0.84612		10	0.45794
3	0.78265		11	0.41144
4	0.64564		12	0.32865
5	0.55461		13	0.29454
6	0.55207		14	0.28401
7	0.53659		15	0.28327

Confidence Limit Correction Factors

Tallies averaged during the active cycles of a Monte Carlo criticality calculation are correlated with each other, since the fission bank used in one cycle was built from the results of the previous cycle. Therefore, the standard confidence interval formula for the tally mean \bar{X} ,

$$\sigma_{\bar{X}}^{app} = \sqrt{\frac{1}{N} \sum_{n=1}^N X_n^2 - \bar{X}^2},$$

underestimates the standard deviation, as we effectively have less samples due to the inter-cycle correlation. The true standard deviation is as follows,

$$\sigma_{\bar{X}}^{true} = \sigma_{\bar{X}}^{app} \sqrt{1 + 2 \sum_{j=1}^{\infty} r_j},$$

where

$$r_j = \frac{E[(X_n - \bar{X})(X_{n+j} - \bar{X})]}{E[(X_n - \bar{X})^2]},$$

are the lag-j correlation coefficients. To approximate the lag coefficients greater than one, Ref. [10] begins with the expected power sum,

$$E[(X_n - \bar{X})(X_{n+j} - \bar{X})] = \rho_1^j E[\eta_1^2] + \rho_2^j E[\eta_2^2] + \dots,$$

$$\rho_i = \frac{k_i}{k_0}.$$

Here $E[\eta_i^2]$ is the expectation of square of the fluctuations in the tally due to the i^{th} mode. Ref. [10], using the dominance ratio, then assumes that the lag-j coefficients decay with powers of the dominance ratio:

$$r_j \approx \rho_1^{j-1} r_1,$$

$$\Rightarrow \sigma_{\bar{X}}^{true} \approx \sigma_{\bar{X}}^{app} \sqrt{1 + \frac{2r_1}{1 - \rho_1}}.$$

This is a conservative approximation (overestimate) to the expected formula for the lag correlation coefficients. The root term is called the MacMillan correction factor. With the fission matrix tallied on a fine enough spatial mesh, we now have additional eigenvalue information. We assume every eigenmode contributes equally to tally fluctuation:

$$E[\eta_1^2] \approx E[\eta_2^2] \approx \dots \approx E[\eta^2],$$

and then use the tallied lag-1 correlation coefficient and spectrum to solve for this constant:

$$E[\eta^2] = \frac{r_1}{\rho_1 + \rho_2 + \dots},$$

to get another approximation for lag correlation coefficients greater than one:

$$r_j \approx \frac{r_1}{\rho_1 + \rho_2 + \dots} (\rho_1^j + \rho_2^j + \dots),$$

$$\Rightarrow \sigma_{\bar{x}}^{true} \approx \sigma_{\bar{x}}^{app} \sqrt{1 + \frac{2r_1}{\sum_i \rho_i} \sum_i \frac{1}{1 - \rho_i}}.$$

The root term above is called the spectrum weighted correction factor. Fig. 32 plots the two space-dependent correction factors along with the empirical correction factors for a simple 40 cm, 1-group, 1D slab problem ($\Sigma_t = 1.0 \text{ cm}^{-1}$, $\Sigma_f = 0.2 \text{ cm}^{-1}$, $\Sigma_c = 0.3 \text{ cm}^{-1}$, $\Sigma_s = 0.5 \text{ cm}^{-1}$, $v = 2.4$, isotropic scattering). We see that using the spectrum gives use correction factors closer to reality, but still conservative. These are promising results, which should be tested on more realistic problems. In theory [18] it is possible to directly calculate correction factors by also using adjoint eigenvectors, but we have not gotten good results, as many complicated calculations are involved. Ref. 19 suggests that the $E[\eta_i]$ terms are proportional to integrals of forward eigenvectors. We tried using this information to improve estimates of the terms, but did not find significant improvements in the correction factors.

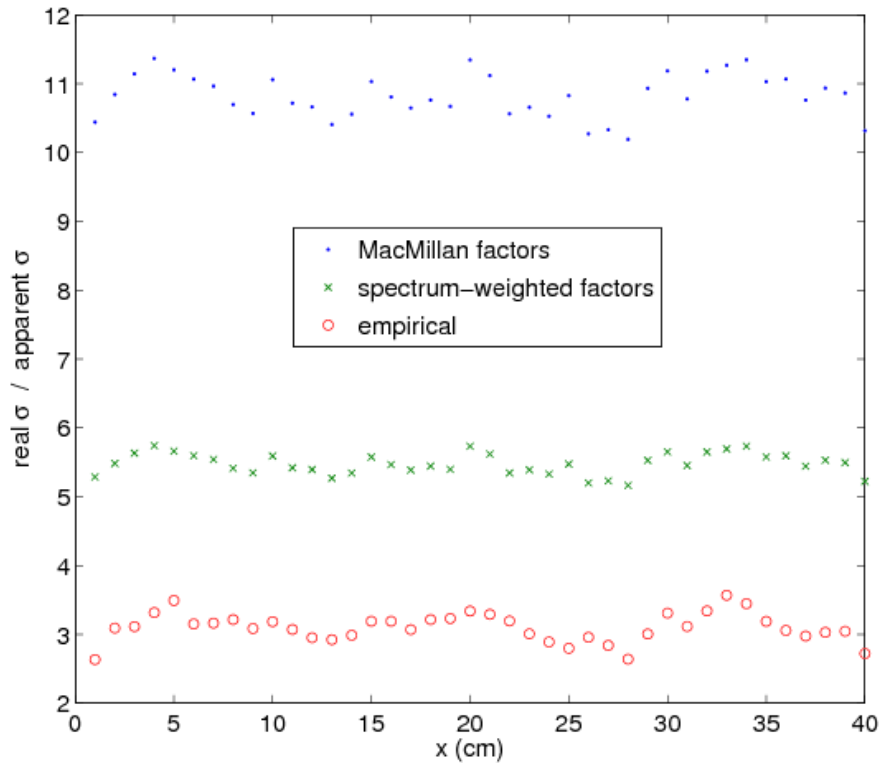


Fig. 32. MacMillan and spectrum weighted correction factors, along with empirical results for a 1D, 1-group problem.

Evaluation of Discretization Error

Analyzing eigenvectors from fission matrices tallied for single cycles is a way to evaluate the effect of the non-exact stochastic fission source. Over the course of all cycles, if there is noticeable correlation between the fission bank and fundamental eigenvector of the fission matrix tallied from the transport of that fission bank, then the meshing is too coarse. Ideally, fission matrix tallying is independent of the fission bank.

Fig. 33 shows single-cycle fission matrix fundamental eigenvector Shannon entropies for a 1D, 40cm, one-group problem ($\Sigma_t = 1.0 \text{ cm}^{-1}$, $\Sigma_f = 0.2 \text{ cm}^{-1}$, $\Sigma_c = 0.3 \text{ cm}^{-1}$, $\Sigma_s = 0.5 \text{ cm}^{-1}$, $\nu = 2.4$, isotropic scattering), with 40 spatial bins. Two batch sizes are plotted. The first noticeable aspect is the overall independence of entropy with cycle number, even though the fission bank becomes more accurate over time (converges in about 100 cycles). This demonstrates the sufficient fineness of the spatial mesh.

A weakly sampled fission matrix, in this case, almost always gives a fundamental eigenvector with high Shannon entropy. This is seen for more complicated problems also; all observed cumulative fission matrix eigenvector entropies start low and rise. This suggests inadequate sampling of the fission kernel usually leads to an equilibrium fission rate distribution lacking in the homogeneity and smoothness of the true fundamental eigenvector, at least for the problems here.

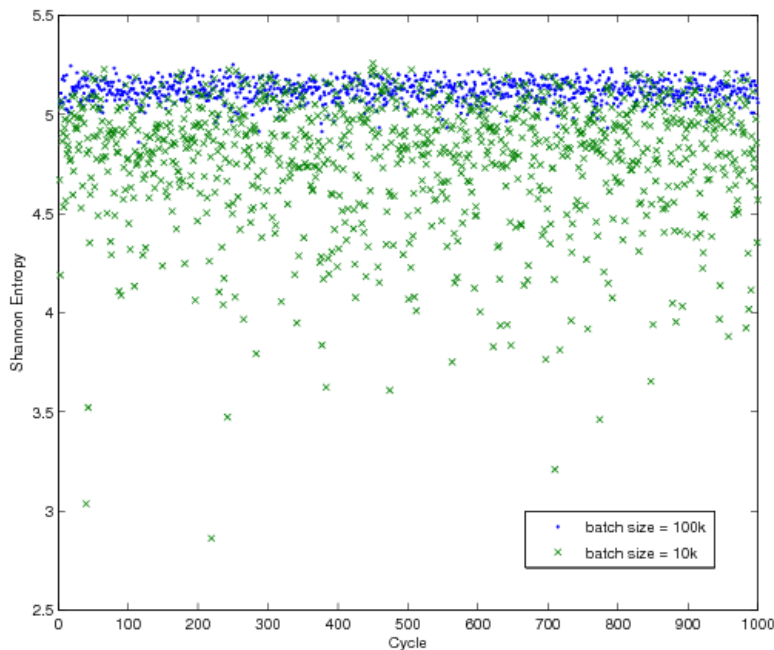


Fig. 33. Single-cycle fission matrix eigenvector Shannon entropy for 100k and 10k batch sizes. 1D, 1-group problem, 40 cm, 40x1x1 spatial mesh, 1000 cycles ran.

Two similar plots, Figs. 34 and 35, show absolute Shannon entropy differences (reference is the final cumulative fission matrix eigenvector) from cycle-wise Monte Carlo/fission matrix eigenvectors for two different meshes on the 2D PWR problem. As stated previously, for a fine enough mesh there should be

no noticeable correlation between the fission bank and resulting fission matrix eigenvector. This is true for the 30x30x1 spatial mesh, but not for the 10x10x1 spatial mesh; in the very first cycle we see that the near-flat fission bank results in a similarly flat fission matrix eigenvector. The correlation coefficients (0 = uncorrelated, -1,1 = perfect correlated) for the two different Shannon entropy trends are -0.03 and 0.26 for the fine and coarse mesh. These numbers make sense and agree with the figures; the coarse fission matrix eigenvector depends on the fission bank shape, thus requiring more skipped cycles before fission matrix tallying can begin. The finer mesh eigenvectors give a correlation coefficient of almost zero, meaning few skipped cycles are required.

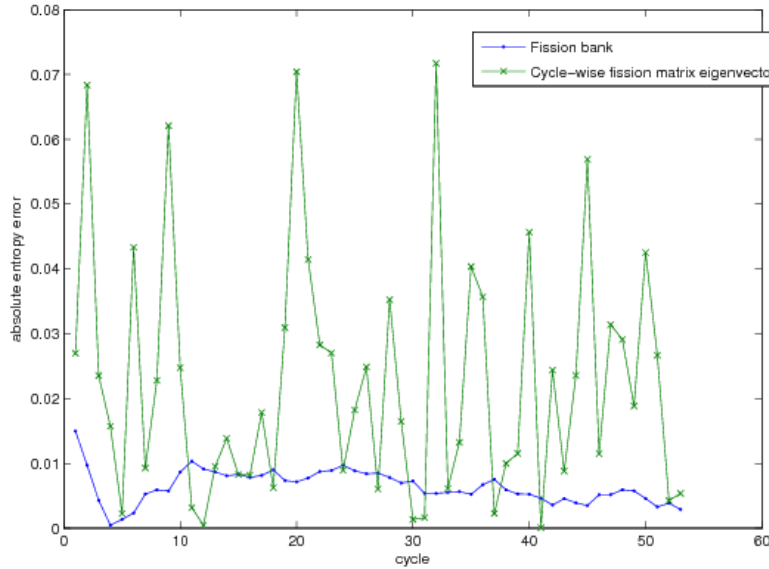


Fig. 34 Absolute Shannon entropy errors for single-cycle fission bank and eigenvector of fission matrix tallied from single-cycle fission bank. 2D PWR problem, 30x30x1 spatial mesh, 500 k batch size.

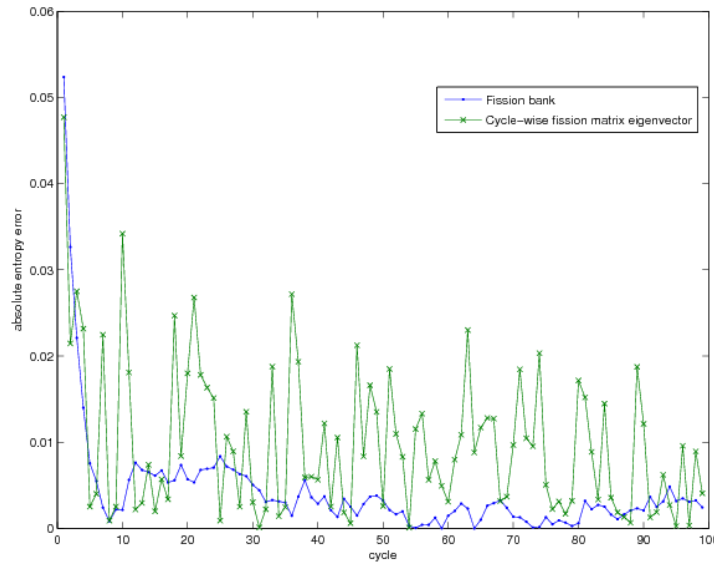


Fig. 35 Absolute H_{src} errors for single-cycle fission bank and eigenvector of fission matrix tallied from single-cycle fission bank. 2D PWR problem, 10x10x1 spatial mesh, 500 k batch size.

This type of evaluation is not great for practical use—another lagged cumulative fission matrix has to be stored.

Nonlocal Exponential Extrapolation

We attempt here to exponentially extrapolate the fission matrix numerator outside of the local region. For every fissionable mesh region in the problem, a least-squares exponential function is calculated using every nonlocal fission weight and fission distance (in units of region-lengths). Storage requirements are $\sim 8N$: five least squares parameters, total nonlocal weight, maximum nonlocal fission distance, and two exponential fit constants. The extent of these fits is limited by the maximum fission distance for the given origin region, and the multiplicative constant is chosen so the total nonlocal fission weight for each origin region is preserved.

$$FM \text{ numerator}(i, j) = \frac{FM \text{ denominator}(i)}{\text{mean}(FM \text{ denominator} \in i_{nl})} \text{Exp}(-\text{dist}(i, j)c(j)),$$

$$i_{nl} = \{i, \text{outside local region of } j \text{ and } \text{dist}(i, j) \leq \max(\text{dist}(i, j)) \text{ for all } j\},$$

$$\text{dist}(i, j) = \sqrt{(n_i - n_j)^2 + (n_i - n_j)^2 + (n_i - n_j)^2}.$$

The origin-dependent exponential constant $c(j)$ is calculated to preserve the total nonlocal fission weight tallied for region j . The multiplicative constant is then given a spatial-dependence by the estimated fissionability of each region, taken from the accumulated fission matrix denominator.

For a homogenous 1D and 2D problem, results from extrapolation were more accurate than any other nonlocal handling scheme tried. Extrapolation inaccuracies grew as distance increased, mostly as underestimation, due to diffusion, or “buildup” in shielding terminology. Errors could be mitigated with quadratic least squares fit as opposed to just linear, but this increases storage by an additional $3N$.

This did reasonably well in a checkerboard problem with highly enriched uranium/low-enriched uranium (HEU/LEU), where fission matrix elements highly depend on destination region enrichments.

Table 5 shows results for a 15x15x1 highly enriched uranium/low-enriched uranium (HEU/LEU) checkerboard problem, with a 30x30x1 spatial mesh. Fission matrix elements highly depend on destination region enrichments. To test the extrapolation, the local region is set so $\sim 13\%$ of fissions are lost. In addition to the extrapolation described above, two other methods are tested. An exponential extrapolation without a destination-dependent multiplicative constant is tested ($c(j) \rightarrow c$). Disregarding nonlocal fission is also tried. Comparing the fundamental eigenvalues in Table 5 shows that disregarding nonlocal fissions and moving to the local region give about the same bias, and exponential fits are slightly more accurate. With regards to source shape, throwing out gave a better shape than moving to closest region. This is understandable given the high nonlocal fraction; far too many nonlocal fissions are moved to the edge of the local region. The exponential fit with fissionability information gives the best source shape. Without the fissionability information the exponential fit gave a bad shape.

Table 5. Fundamental eigenvalue and eigenvector accuracies for different nonlocal handling methods

	K_{eff} % difference from full fission matrix	Shannon entropy % difference from full fission matrix
Disregard nonlocal	2.58	-0.76
Put on closest local region	2.58	1.64
Exp. fit	-0.51	2.66
Exp. fit with fission matrix denominator-dependent constant	1.04	-0.32

Because there is little accuracy gained from this fit relative to simpler nonlocal handling methods, and more storage/work is required, this scheme is not pursued further.

Track length Estimator

We implemented a track length estimator of the fission matrix by modifying the track length mesh tally in the MCNP `fmesh_mod` routine. Finding the extent of the statistical advantage is of primary interest—the entire random walk is now used for tallying, as opposed to just the start and finish. Due to the nontrivial overhead of this estimator, we require a significant statistical benefit for serious consideration of use. The extra work required is greatest in Message Passing Interface (MPI) runs, since gathering potentially large (GBs) fission matrices across nodes is required for eigen decomposing. Regardless of parallel considerations is the loss of simplicity-- fission bank use for tallying requires no significant additions to the standard criticality calculation. The final motivation for track length implementation is verification—finding agreement with the fission bank estimator in the limit of zero variance.

This paragraph details implementation considerations. The `fmesh` input card requires meshing parameters that match the entropy grid, and no energy bins are specified. The macroscopic $v\Sigma_f$ tally multiplier is required (`fm# -1.0 0 -6 -7`), which makes the tally a fission reaction rate estimator. Most extra work required in the `fmesh` module is the determination of the fission matrix indices to which reaction rate scores are added. When a new history is started, the origin region index is saved. A new history is identified by saving and comparing the `npstc` value each time the subroutine `mesh_score` is called. The sparse storage scheme is used here; the special `fmesh` tally is allocated to the local region size by the number of regions. Whereas the standard `fmesh` tally is allocated in the following manner: `(nx,ny,nz,# of energy groups, ntasks+1)`, the fission matrix tally is allocated as `(local region size, nx*ny*nz,1,1,ntasks+1)`.

Any nonlocal fission handling scheme used by fission bank estimation is possible with this estimator, though only adding to the closest local fissionable region is implemented. In `fmatrix_mod`, the ID of the `fmesh` tally is found, and the tally is used directly in the matrix solve routine after being normalized by the fission matrix denominator (found from fission bank). Following the matrix solve, the tally is then unnormalized to again represent the numerator.

The track length estimator is tested on the OECD/NEA source convergence benchmark fuel storage vault problem and the 2D PWR problem. In the fuel vault problem, 16 regions per assembly are used, with no meshing in the z-direction (96x12x1 spatial mesh). Two cycles are skipped for fission matrix tallying,

with a 1 M batch size. No sparse approximation is used. Fission bank tallying took four cycles for the eigenvector to be properly peaked at the top left, whereas track length tallying is properly peaked after one. Fig. 36 compares the two estimators along with the Monte Carlo results. Track length estimation took 4.7 computer-hours per kcode cycle, as opposed to 2.8 computer-hours per cycle for fission bank tallying (both ran with 16 threads, no mpi). We see the desired agreement between the two estimators for long times.

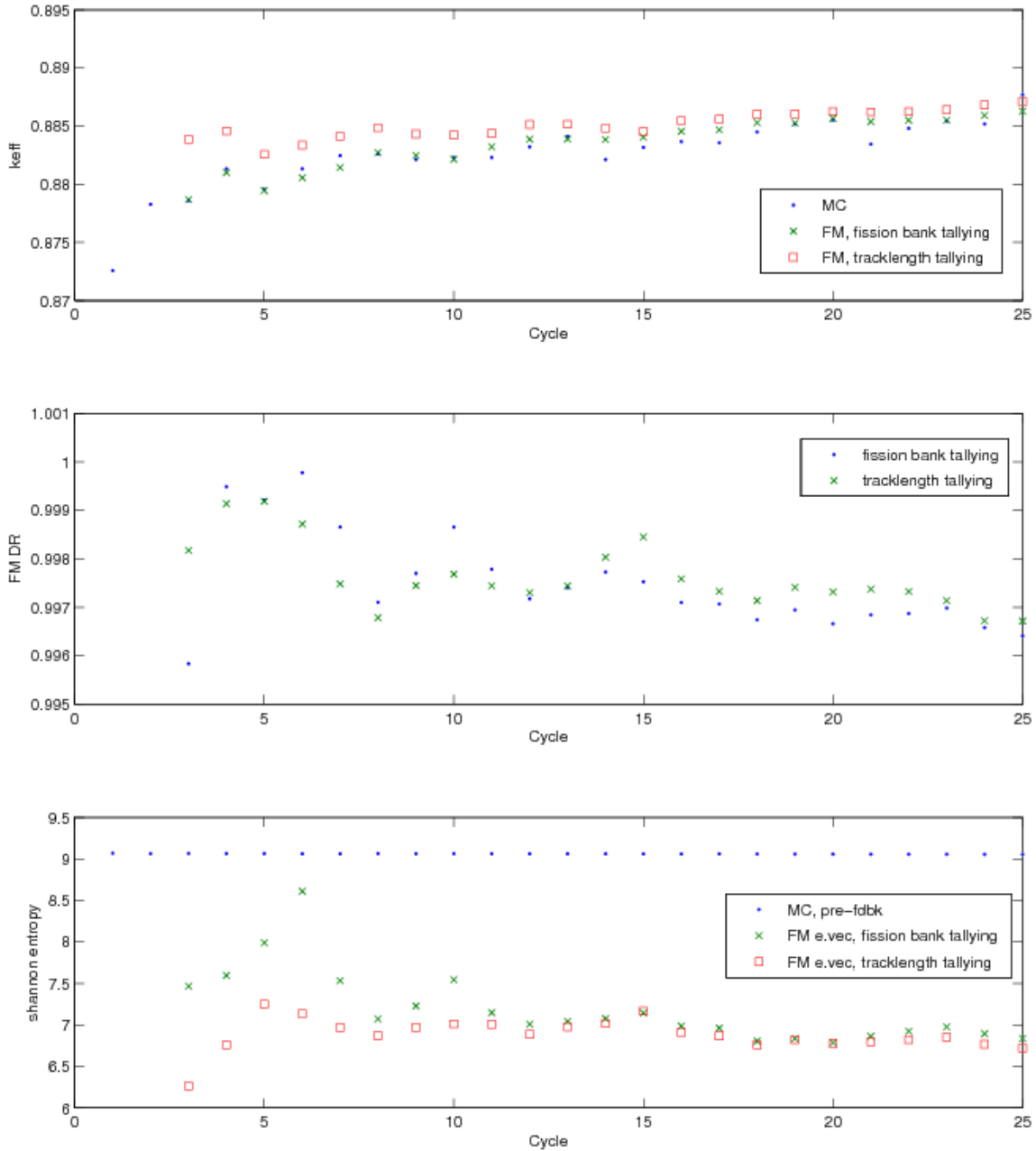


Fig. 36. k_{eff} , dominance ratio, and Shannon entropy convergence behavior for Monte Carlo, fission matrix with fission bank tallying, and fission matrix with track length tallying for fuel storage vault problem, 96x12x1 spatial mesh.

In the 2D PWR problem, 16 regions per assembly are again used (60x60x1 spatial mesh). Fission matrix tallying began at the 4th cycle, and sparse storage is used, with a local distance of two assembly lengths, resulting in about 0.5% fissions being nonlocal. The batch size is 500 k. Fig. 37 compares the two tallies, and a lesser improvement occurs in this easier problem. Track length estimation took 4.2 computer-hours per k code cycle, as opposed to 3.8 computer-hours per cycle for fission bank tallying (16 threads with no MPI for both runs). We again see long-term agreement.

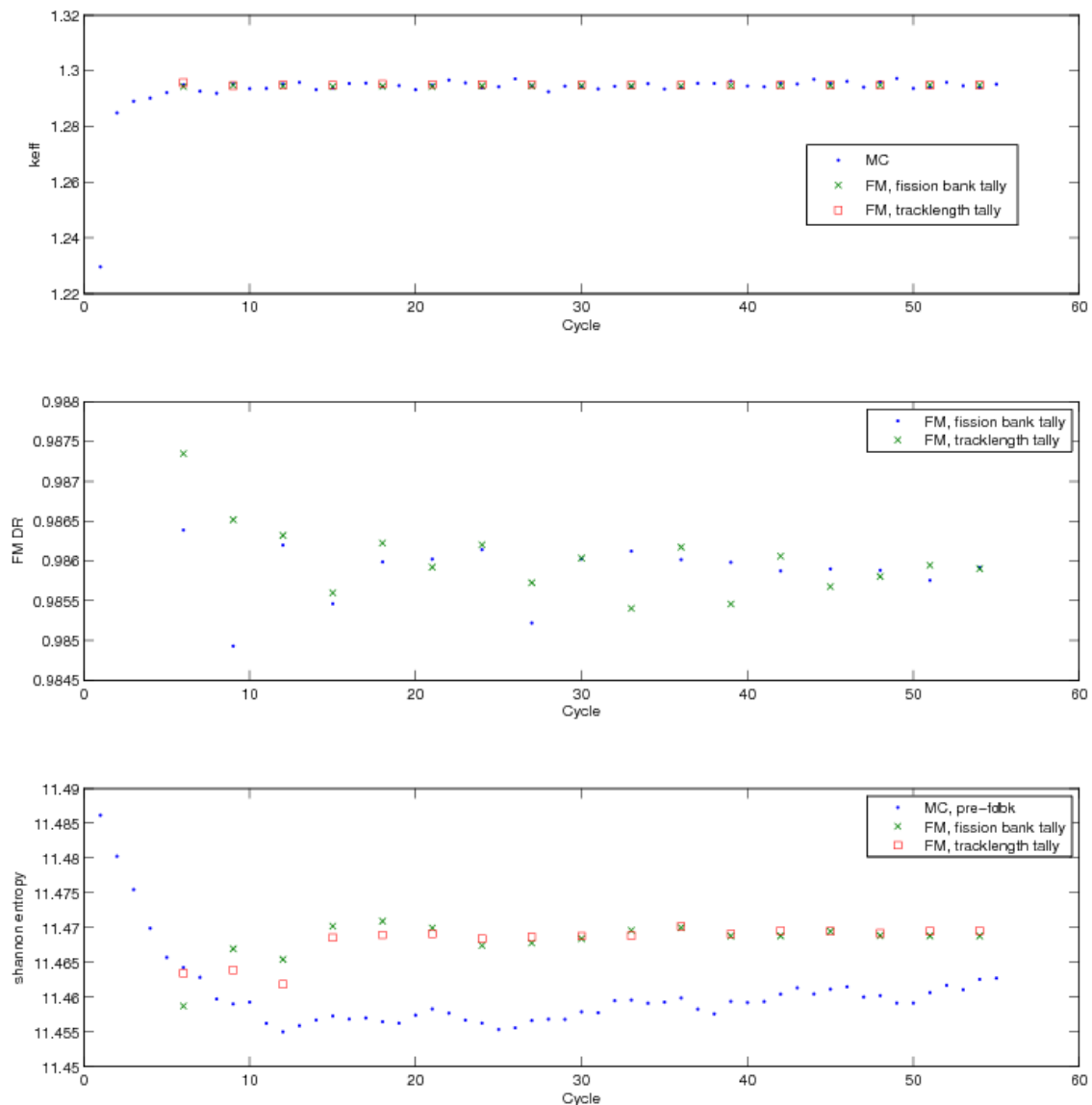


Fig. 37. k_{eff} , dominance ratio, and Shannon entropy convergence behavior for Monte Carlo, fission matrix with fission bank tallying, and fission matrix with tracklength tallying for 2D PWR problem, 60x60x1 spatial mesh.

From the two problems tested, the track length estimator is more statistically efficient, but not enough so to warrant the additional complexity and longer runtime. In 3D problems with very fine meshing, though, advantages should be larger. Nevertheless, the results from this evaluation support the use of the fission bank.

Convergence Evaluation

The determination of source convergence is a challenge for Monte Carlo eigenvalue calculations. While metrics like Shannon entropy can characterize the fission source, the stochastic effects prevent the use of simple convergence evaluations that are used in deterministic methods. Post-run evaluation of Shannon Entropy can be sufficient for convergence evaluation, but this requires storage of all quantities of interest for every cycle. When tallies are multitudinous, such as in pin-power tallies, this can become too memory-intensive. With the availability of the fission matrix fundamental eigenmode, an anchor is provided from which fission bank convergence can be evaluated easier.

A cumulative estimation of the fission kernel allows for an eigenvector that has a more stable convergence, similar to what is seen in deterministic methods. Stochastic effects are damped due to the benefit of using cumulative tallies to find the eigenvector. Disregarding the minor sampling and sparsification bias, this converged eigenvector can be treated as correct on its level of spatial detail. With this low-order solution, it is now possible to declare fission bank convergence with much greater confidence. False convergence issues in high dominance ratio problems can be better avoided.

Evaluation of the fission matrix fundamental eigenvector convergence is necessary before it is used. Three options are considered: max root-mean-squared change of a single eigenvector element, relative L2 norm change, and relative entropy:

$$\text{max rms change} = \max_i \sqrt{(S_{i,c})^2 - (S_{i,c-1})^2} ,$$

$$\text{relative L2 norm change} = \frac{\|S_c - S_{c-1}\|_2}{\|S_{c-1}\|_2} ,$$

$$FM, \text{Relative Shannon Entropy} = h_{src,rel} = - \sum_{i=1}^N \frac{S_{i,c}}{\|S_c\|_1} \log_2 \left(\frac{S_{i,c} / \|S_c\|_1}{S_{i,c-1} / \|S_{c-1}\|_1} \right) \leq 0 ,$$

$$FM - MC, \text{Relative Shannon Entropy} = - \sum_{i=1}^N \frac{S_{i,MC}}{\|S_{MC}\|_1} \log_2 \left(\frac{S_{i,MC} / \|S_{MC}\|_1}{S_{i,FM} / \|S_{FM}\|_1} \right) \leq 0 ,$$

where

$$i = \text{spatial index} ; c = \text{cycle index} .$$

Others [15] have used a relative L1 norm change of 0.05 for determining fission matrix eigenvector convergence. Figs. 38, 39, 40, and 41 show these metrics for the 2D PWR, Kord Smith Challenge, fuel storage vault, and ATR. We see that the max rms change, relative L2 norm change, and relative entropy of consecutive fission matrix eigenvectors behave similarly; both begin exponentially converging and eventually approach a constant change. The salient metric is the relative entropy of the fission bank with reference being the fission matrix eigenvector. Figs. 38 and 39, the reactor problems, have a sharp plateau, from which fission bank convergence can be gleaned. In the fuel storage vault problem, even at cycle 200 the fission bank is far from being converged, while the fission matrix eigenvector quickly converges. For relative entropy to be a beneficial fission bank convergence metric, it should be clear when the source is not converged. In addition to the visual lack of convergence in the relative entropy plot, the actual values are large compared with the reactor cases. Therefore, we have clear indicators that the fission bank is not converged.

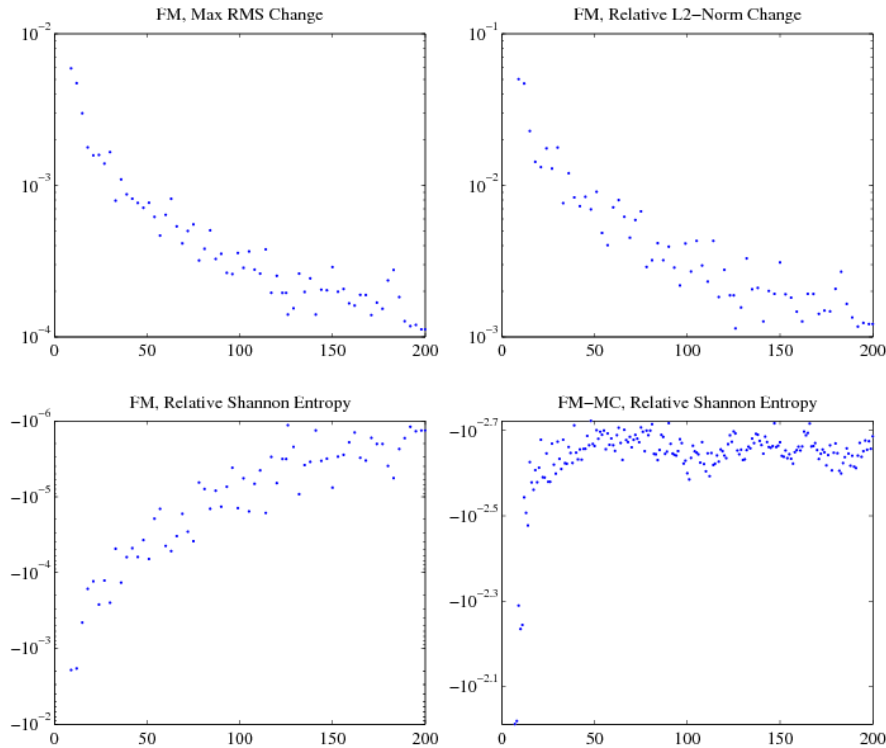


Fig. 38 Various eigenvector convergence criteria, 2D PWR, 30 by 30, 500k batch size, fission matrix tallying begins cycle 4, solved every 3 cycles

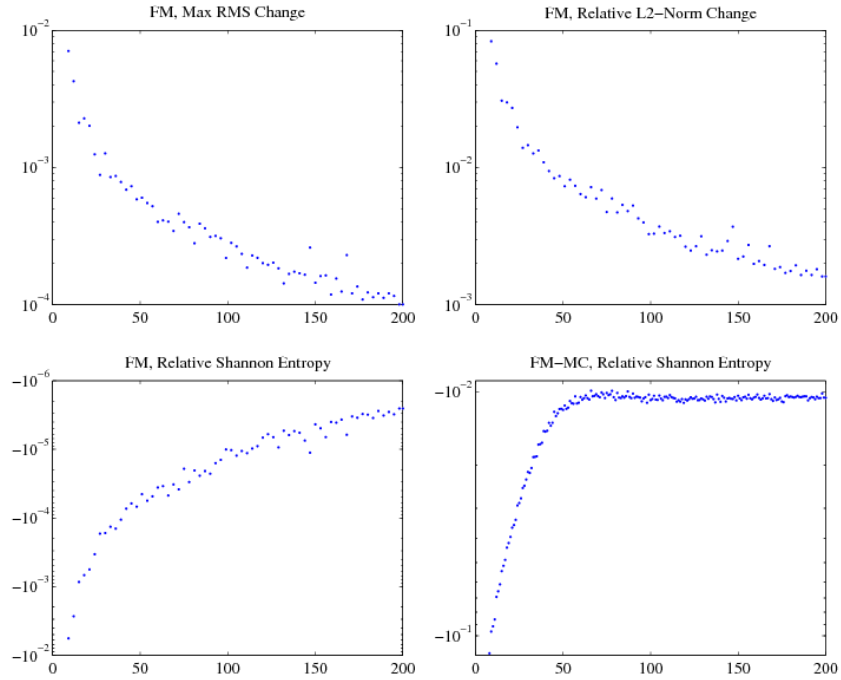


Fig. 39 Various eigenvector convergence criteria, 3D Kord Smith Challenge Problem, 21 by 21 by 20, 1M batch size, fission matrix tallying begins cycle 4, solved every 3 cycles

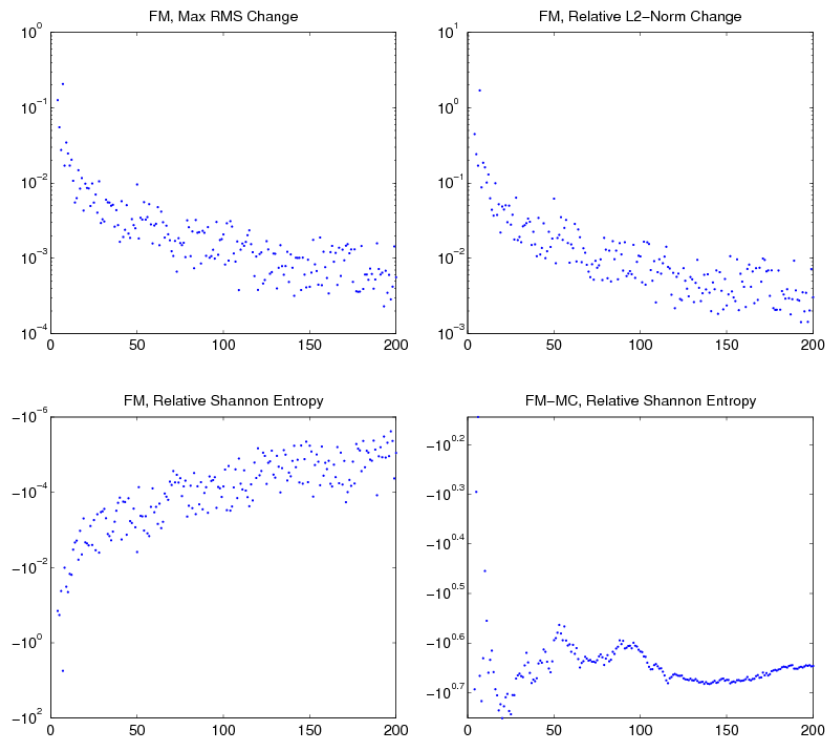


Fig. 40 Various eigenvector convergence criteria, Fuel Storage Vault Problem, 96 by 12 by 10, 1M batch size, fission matrix tallying begins cycle 3, solved every cycle

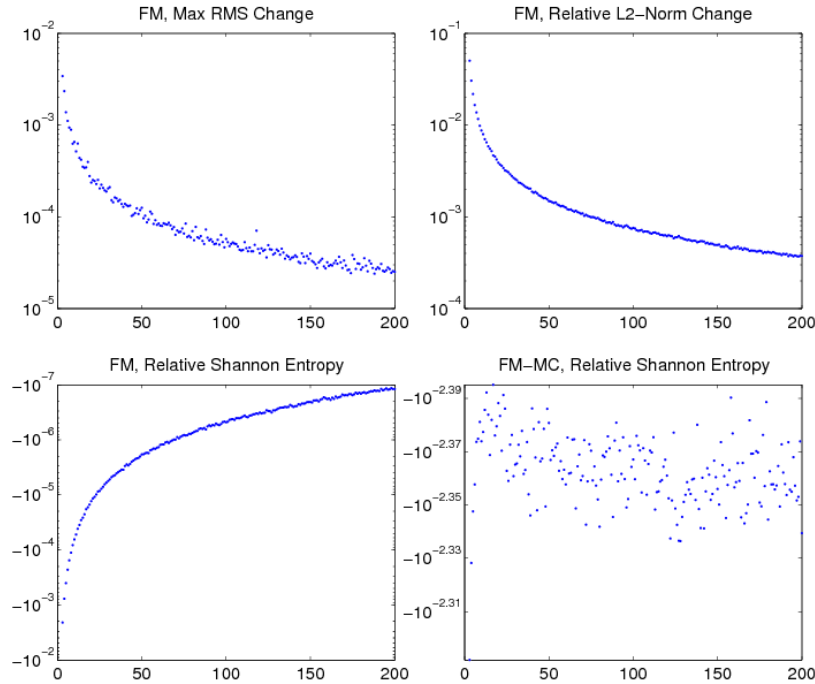


Fig. 41 Various eigenvector convergence criteria, ATR Problem, 100 by 100, 1M batch size, fission matrix tallying begins cycle 2, solved every cycle

Conclusions

We have applied the fission matrix method mainly to four realistic problems: 2D PWR, 3D Kord Smith Challenge, fuel storage vault, and ATR. We found excellent source converge acceleration for the two hardest problems: Kord Smith Challenge and fuel storage vault. While regular Monte Carlo in both problems converged at around cycles 50 and 2000, respectively, the fission matrix fundamental eigenvector converged at cycles 7 and 30.

We also examined the higher eigenmodes and eigenvalues. We found spectrum convergence for increasingly fine meshing, and empirical evidence showing that imaginary components of the eigenvalue spectrum are a result of noise. Certain eigenmodes showed multiplicity for the PWR problems. Using quarter-core and half-core models for a homogenous reactor problem, we saw the elimination of non-symmetric modes. Using part of the eigenvalue spectrum for a one-group 1D problem, we found confidence interval correction factors that improved over existing corrections [10]. While empirical correction factors were around 3, MacMillan correction factors, large overestimations, were around 11. Using part of the eigenvalue spectrum from the fission matrix, we found more accurate factors of around 5.5.

We also found near-orthogonality of eigenfunctions for all problems tested. This implies the near-symmetry of the fission matrices. This observation suggests an approximation for source-convergence acceleration. For early cycles, we could assume fission matrix symmetry and add the transpose of the off-diagonal fission matrix to itself. This effectively doubles the amount of tallies by assuming a symmetric

fission kernel. In early cycles, the accuracy gain from this doubling of samples could outweigh the loss in accuracy from the symmetry assumption. No extra memory would be required, nor would existing storage be altered; only the matrix solve routines would have to be modified.

We found the track length estimation of the fission matrix to give lower variances, but not enough to warrant losing the simplicity and quickness of fission bank tallying. By looking at eigenvectors from fission matrices tallied for only single cycles, we were able to declare the 10x10x1 spatial mesh on the 2D PWR problem too coarse, and we found the 30x30x1 mesh to be acceptable. We attempted to exponentially extrapolate the fission matrix numerator outside the local region. While we see improvements over other methods, this extrapolation required significant work, and its effectiveness would be problem-dependent. We also looked at different convergence criteria for the fission matrix and fission bank, and showed that fission bank convergence using the converged fundamental eigenvector of the fission matrix could easily be decided.

Another possible application of the fission matrix is perturbation calculation. If a local cross-sectional change occurs, it should only affect the fission kernel nearby. We can take advantage of this with the fission matrix. All computational effort could go into reevaluating the fission matrix in the local region of the perturbation—quicker than using the unperturbed eigenfunction as an initial guess. There is also the possibility of approximating time-dependent behavior (Boiling Water Reactor power oscillations, Xenon oscillations, control rod movements, fuel burnup, etc.) by functionally expanding the fission source with higher eigenmodes. Modal expansion methods have been developed [20] and applied [21] in terms of neutron flux, and at the moment it is unclear of the applicability of fission source eigenmodes.

References

1. X-5 Monte Carlo Team, “MCNP – A General N-Particle Transport Code, Version 5 – Volume I: Overview and Theory”, LA-UR-03-1987, Los Alamos National Laboratory (2003).
2. L. L. Carter, N.J. McCormick, “Source Convergence in Monte Carlo Calculations”, *Nucl. Sci. Eng.*, **36**, pp 438–441 (1969).
3. G.W. Morrison, J.T. Mihalcz, D.C. Irving, “REACT and CONVRG Fortran Subroutines for Determining Source Convergence for the 05R Monte Carlo Neutron Transport Code”, Oak Ridge National Laboratory, ORNL-TM-1325 (1966).
4. M. R. Mendelson, “Monte Carlo Criticality Calculations for Thermal Reactors”, *Nuc. Sci. and Eng.*, **32**, pp 319-331 (1968).
5. D. E. Kornreich, D. K. Parsons, “Diffusion and Transport Analysis of Higher Mode Eigensystems”, *Nucl. Math. And Comp. Sci. :A Century in Review, A Century Anew* (2003).
6. M. Nakagawa, T. Mori, “Whole Core Calculations of Power Reactors by Use of Monte Carlo Method”, *Nucl. Sci. and Tech.*, **30** [7], pp 692-701 (1993).
7. J.E. Hogenboom, W.R. Martin, B. Petrovic, “Monte Carlo Performance Benchmark for Detailed Power Density Calculation in a Full Size Reactor Core”, *OECD/NEA* (2010).

8. F. B. Brown, R. C. Little, A. Sood, D. K. Parsons, "MCNP Calculations for the OECD/NEA Source Convergence Benchmarks", *Trans. Am. Nucl. Soc.*, **87**, 150 (2003).
9. S. S. Kim, B. G. Schnitzler, et. al., "Serpentine Arrangement of Highly Enrichment Water-Moderated Uranium-Aluminide Fuel Plates Reflected by Beryllium", Idaho National Laboratory, HEU-MET-THERM-022, (2005).
10. D. B. MacMillan, "Monte Carlo Confidence Limits for Iterated-Source Calculations", *Nucl. Sci. and Eng.*, **50**, pp 73-87 (1973).
11. S. Carney, F.B. Brown, B. Kiedrowski, W.R. Martin, "Fission Matrix Capability for MCNP Monte Carlo", *Trans. Am. Nucl. Soc.*, (2012).
12. F.B. Brown, S. Carney, B. Kiedrowski, W.E. Martin, "Fission Matrix Capability for MCNP Monte Carlo", *Nucl. Explosives Code Dev. Conf.*, (2012).
13. J. Dufek, W. Gudowski, "Fission matrix based Monte Carlo criticality calculations", *Ann. Nucl. Energy*, **36**, pp 1270-1275 (2009).
14. M. Wenner, A. Haghghat, "A Fission Matrix Based Methodology for Achieving an Unbiased Solution for Eigenvalue Monte Carlo Simulations", *Prog. In Nucl. Sci. and Tech.*, **2**, pp 886-892 (2011).
15. T. Kitada, T. Takeda, "Effective Convergence of Fission Source Distribution in Monte Carlo Simulation", *J. Nucl. Sci. and Tech.*, **38** [5], pp 324-329 (2001).
16. T. Urbatsch, "Fission Matrix Capabilities in MCNP", Los Alamos National Laboratory, TJU-92-557 (1992).
17. J. Ragusa, "NUEN 489: FA and 3-D core modeling and analysis", *Texas A & M Univ.*, (http://nuclear.tamu.edu/~ragusa/documents/courses/489_09A/lectures/nuen489-Spring09-lecture-14.pdf) Date of access: 8/13/2012.
18. E.M. Gelbard, R.E. Prael, "Monte Carlo Work at Argonne National Laboratory", in Proc. NEACRP Meeting of a Monte Carlo Study Group, Argonne National Laboratory, ANL-75-2 (1974).
19. T. Ueki, F.B. Brown, D.K. Parsons, J.S. Warsa, "Time Series Analysis of Monte Carlo Fission Sources: I.Dominance Ratio Computation", Los Alamos National Laboratory, LA-UR-03-5823 (2003).
20. W.M. Stacey Jr., "Space-time Nuclear Reactor Kinetics" Academic Press, New York (1969).
21. D. Vashee, L. Tayebi, J. Luxat, "Reference Model Parameter Identification of Space-Time Dependent Reactivity in a CANDU-PWHR", *Ann. Nucl. Energy*, **35**, pp 228-237 (2008).

Appendix A

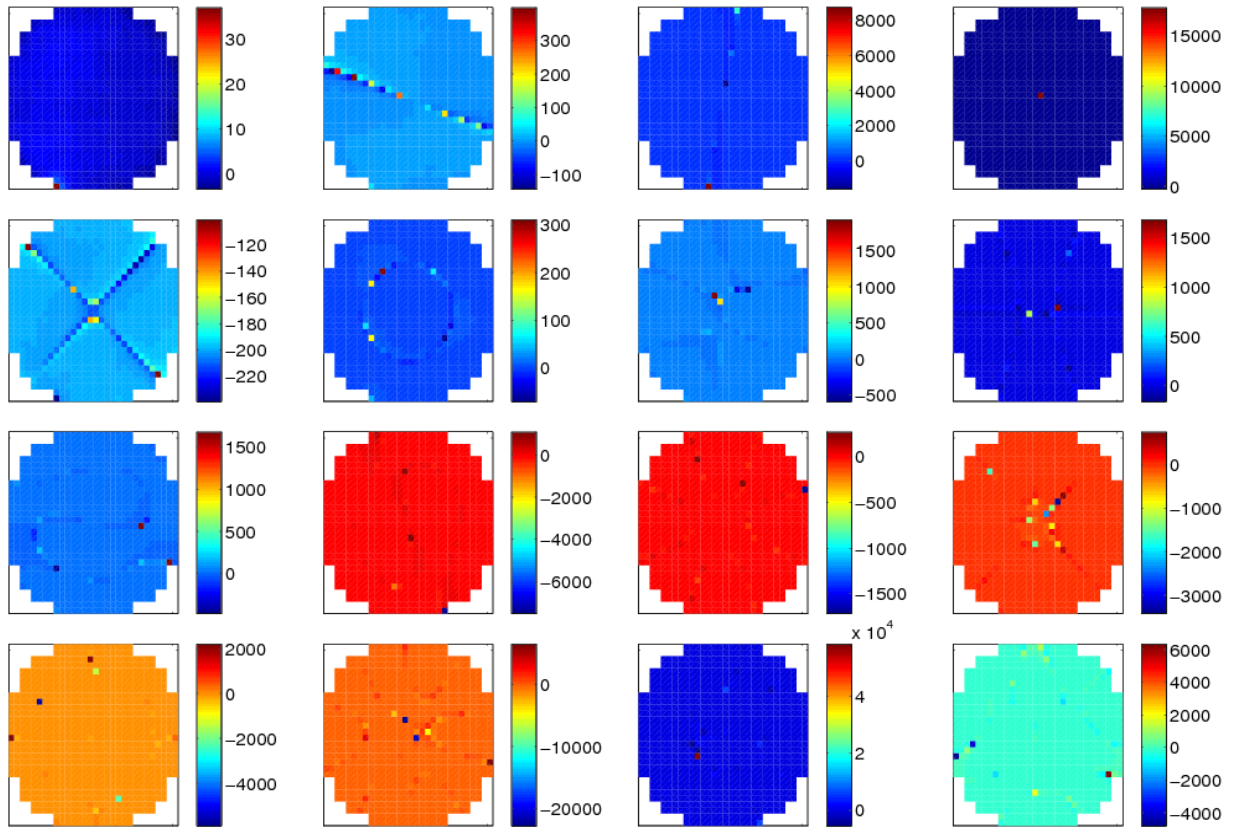


Fig. A.1. Percentage difference in sparse and full 0-15 eigenvectors for the 30x30x1 spatial mesh, 2D PWR problem: $(s_{i,\text{sparse}} - s_{i,\text{full}}) / s_{i,\text{full}}$.

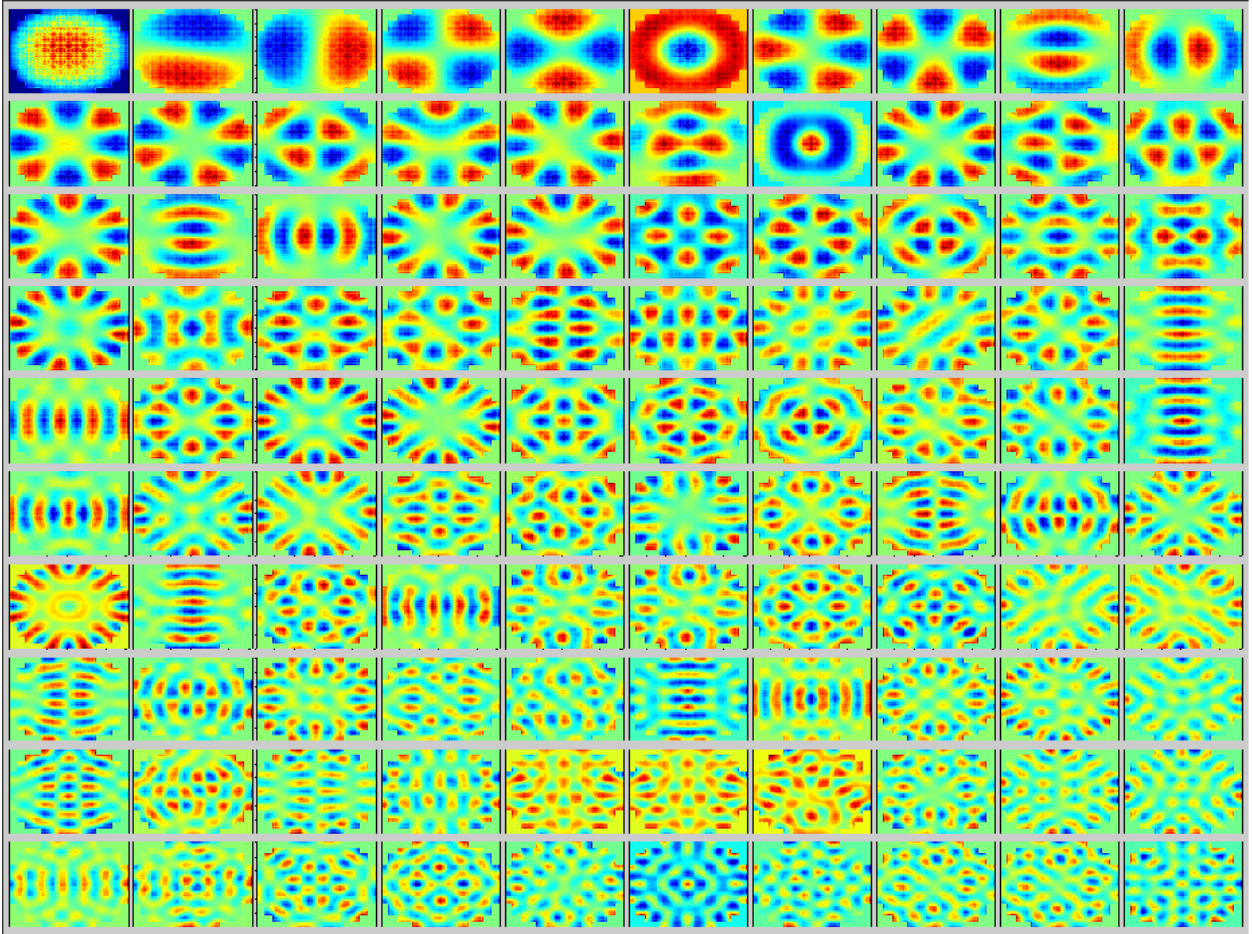


Fig. A.2. First 100 eigenmodes for 2D PWR problem on a 120x120x1 spatial mesh. Fission matrix tallied for 96 cycles with a batch size of 500 k.

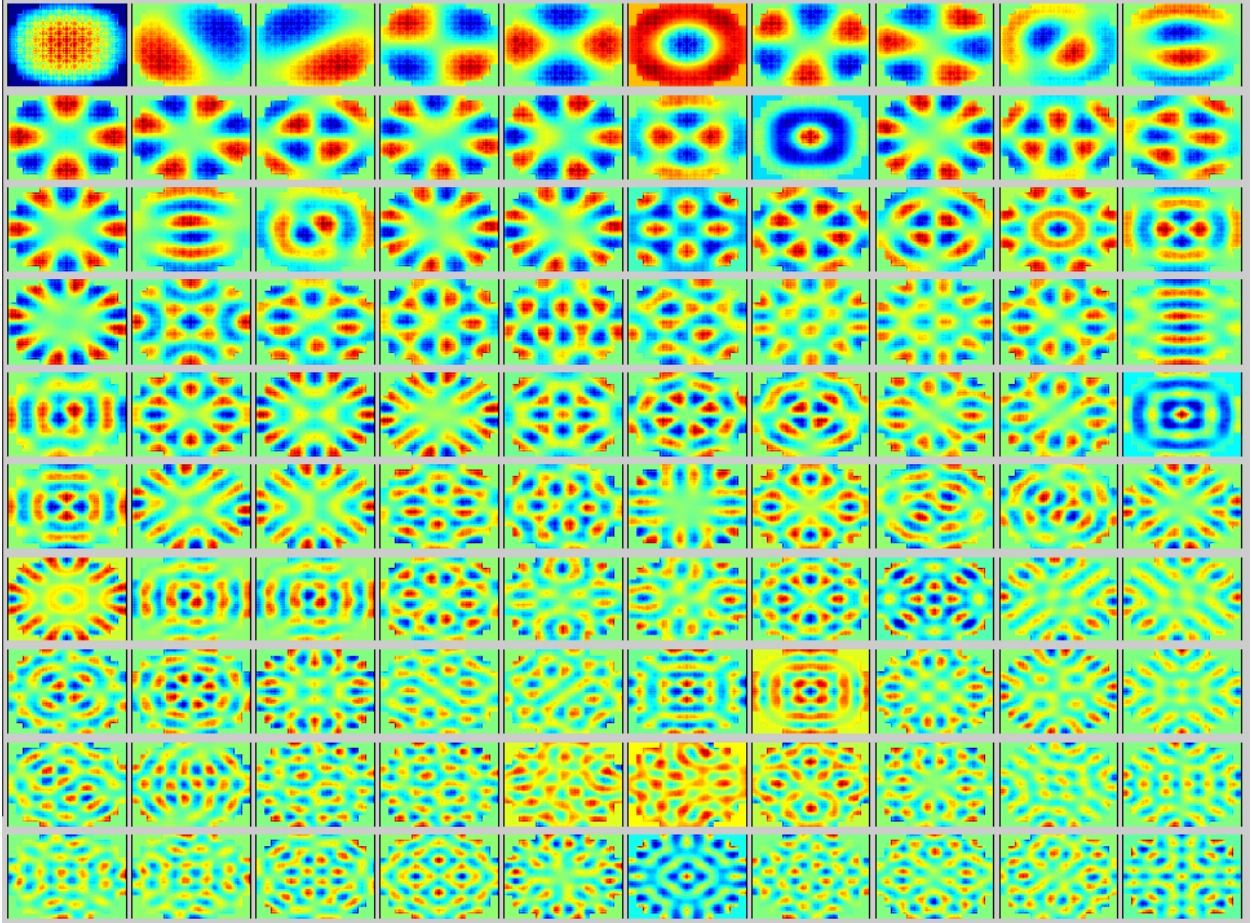


Fig. A.3. First 100 eigenmodes for 2D PWR problem on a 120x120x1 spatial mesh. Fission matrix tallied for 96 cycles with a batch size of 5 M.

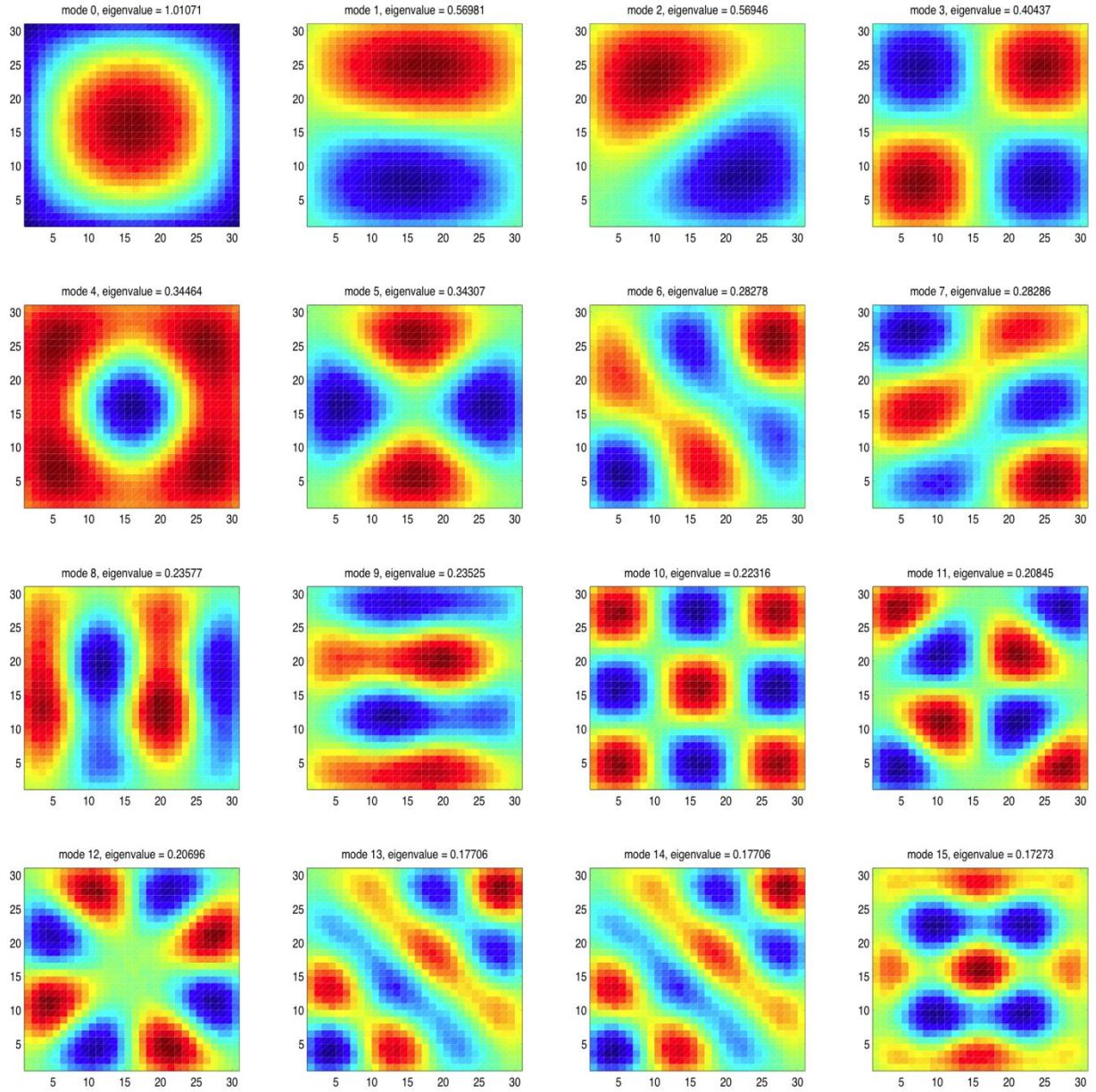


Fig. A.4. Higher eigenmodes for whole-core (30x30x1 spatial mesh) model of 2D homogenous reactor. Fission matrix tallied for 51 cycles, with batch size of 500 k.

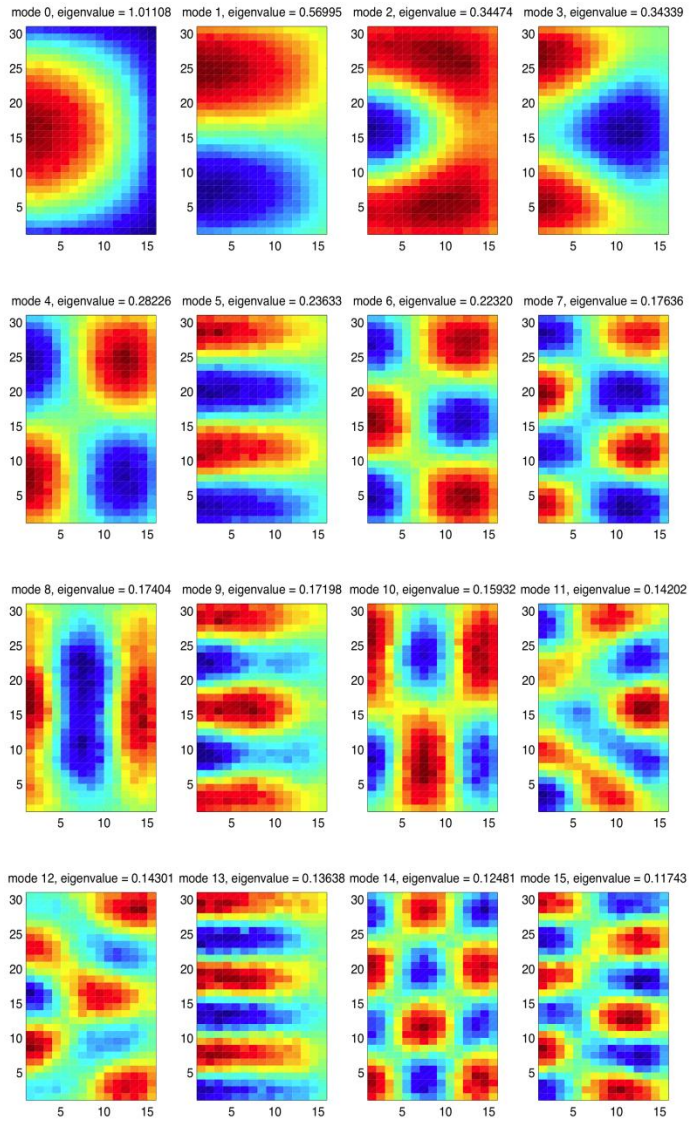


Fig. A.5. Higher eigenmodes for half-core (15x30x1 spatial mesh) model of 2D homogeneous reactor. Fission matrix tallied for 51 cycles, with batch size of 500 k.

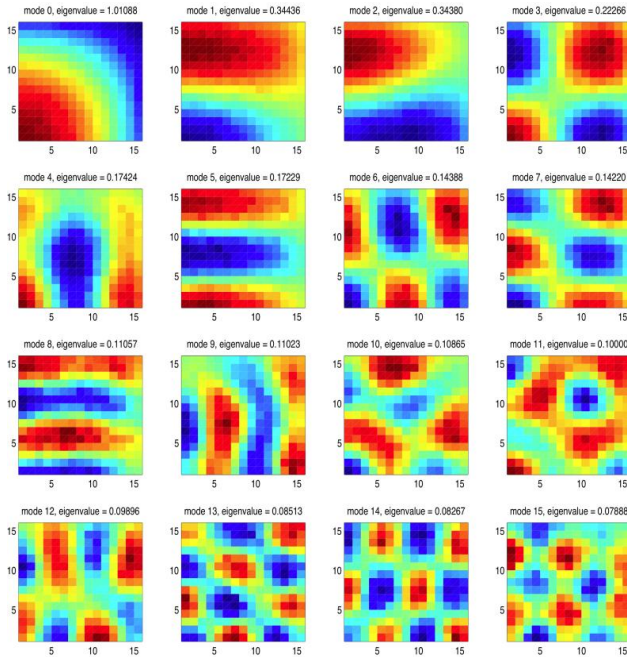


Fig. A.6. Higher eigenmodes for quarter-core (15x15x1 spatial mesh) model of 2D homogeneous reactor. Fission matrix tallied for 51 cycles, with batch size of 500 k.

Appendix B

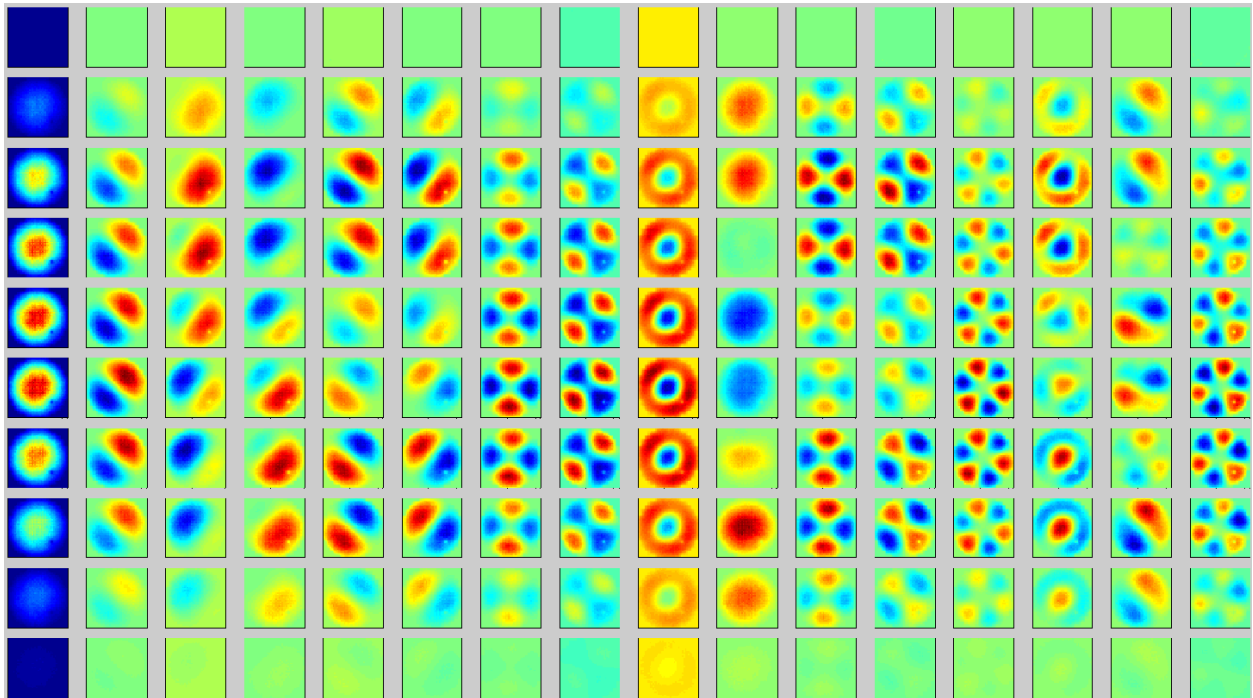


Fig. B.1. First 15 eigenmodes for Kord Smith Challenge with Silver-Indium-Cadmium control rods [17] fully inserted into one assembly., 42x42x20 spatial mesh. Ten XY planes are shown. Fission matrix tallied for cycles 4-200, batch size of 1 M.

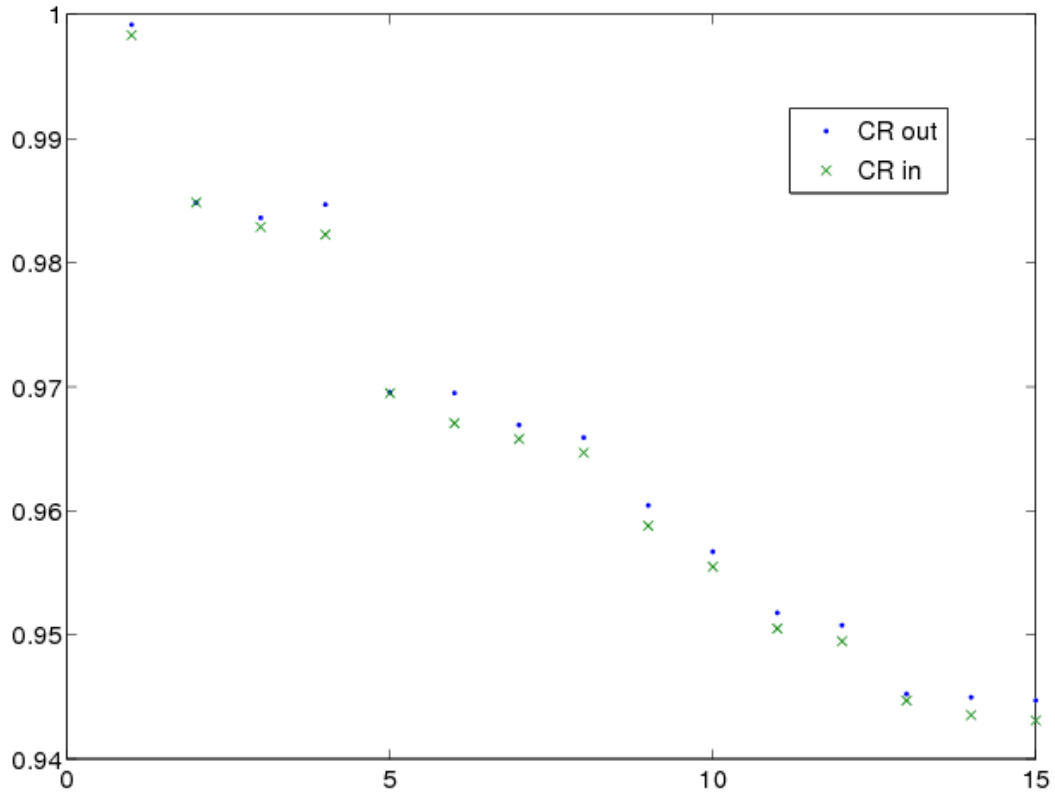


Fig. B.2. First 15 eigenvalues for Kord Smith Challenge with Silver-Indium-Cadmium control rods [17] fully inserted into one assembly., 42x42x20 spatial mesh. Also shown are first 15 eigenvalues with control rod insertion. Fission matrix tallied for cycles 4-200, batch size of 1 M.

Appendix C

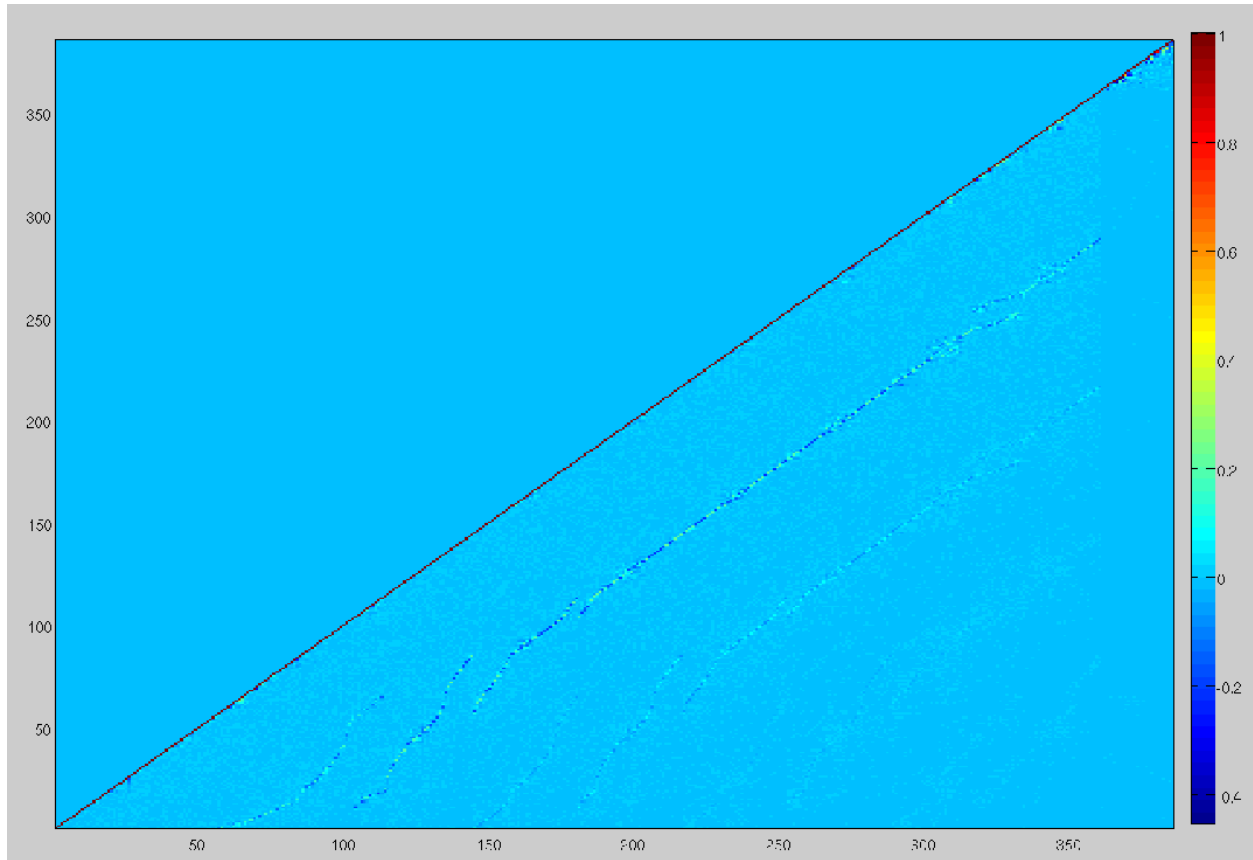


Fig. C.1. Magnitude of inner products ($\#n$ and $\#m$) of first 385 forward eigenfunctions for fuel storage vault problem, 96x12x10 spatial mesh. Fission matrix tallied for cycles 3-200, 1 M batch size.

Appendix D

Figs. D.1-D.8 and Table D.1 show results from an infinite lattice calculation. A single 2.1% enriched assembly from the 2D PWR problem is modeled with periodic boundary conditions. The lattice of fuel pins and water tubes is 17x17 in size, and the fission matrix spatial mesh is 68x68x1, with no sparse approximation. The fission matrix is tallied for cycles 4-300, with a batch size of 500 k.

We see a minor bias in the fission matrix fundamental eigenvector from Fig. D.1. Figs. D.5 and D.6 show the real part of the first 16 eigenvectors from a fission matrix tallied for cycles 4-75 and 4-300. Figs. D.7 and D.8 show the imaginary part. Each eigenmode shows continuity over periodic boundaries.

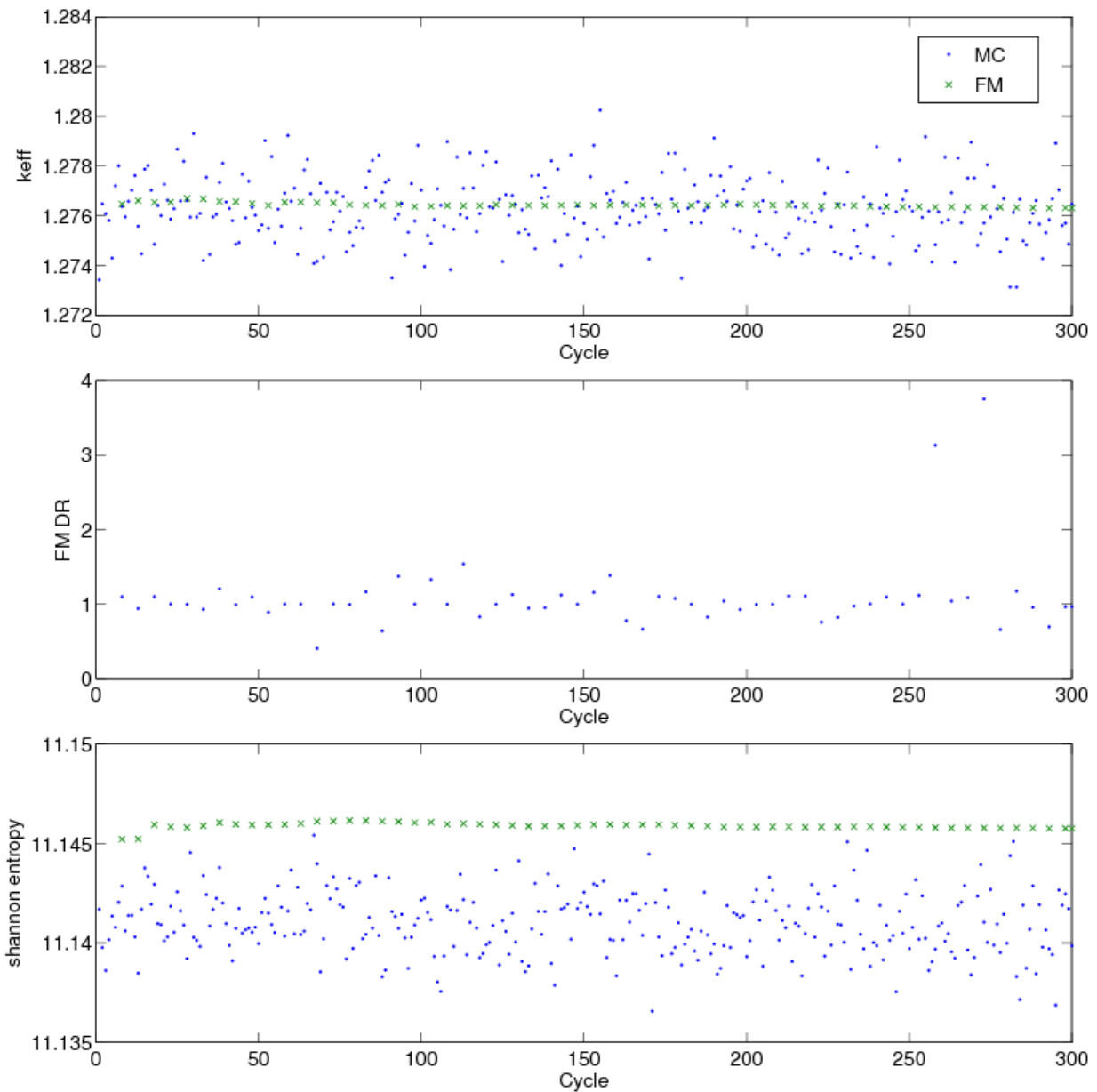


Fig. D.1. Convergence behavior for infinite lattice of 2.1% enriched 17x17 assembly from 2D PWR problem. Fission matrix tallied for cycles 4-300, batch size of 500 k. 68x68x1 spatial mesh.

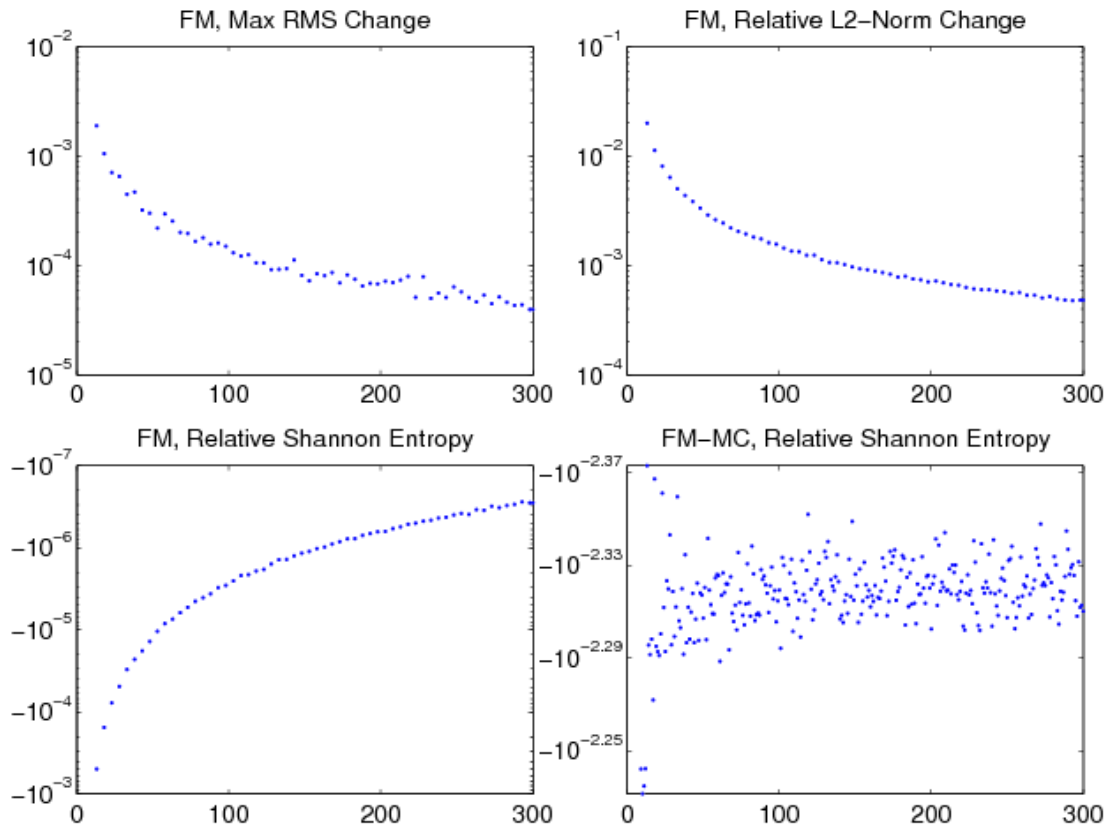


Fig. D.2. Convergence metrics for infinite lattice of 2.1% enriched 17z17 assembly from 2D PWR problem. Fission matrix tallied for cycles 4-300, batch size of 500 k. 68x68x1 spatial mesh.

Table D.1. First 16 eigenvalues for infinite lattice of 2.1% enriched 17z17 assembly from 2D PWR problem. Fission matrix tallied for cycles 4-300, batch size of 500 k. 68x68x1 spatial mesh.

n	k_n	n	k_n
0	1.27630	8	0.03526
1	0.08710	9	$0.02117 + 0.00022i$
2	0.08694	10	$0.02117 - 0.00022i$
3	0.08566	11	$0.02082 + 0.00021i$
4	0.08549	12	$0.02082 - 0.00021i$
5	0.03614	13	0.01938
6	$0.03569 + 0.00014i$	14	$0.01920 + 0.00030i$
7	$0.03569 - 0.00014i$	15	$0.01920 - 0.00030i$

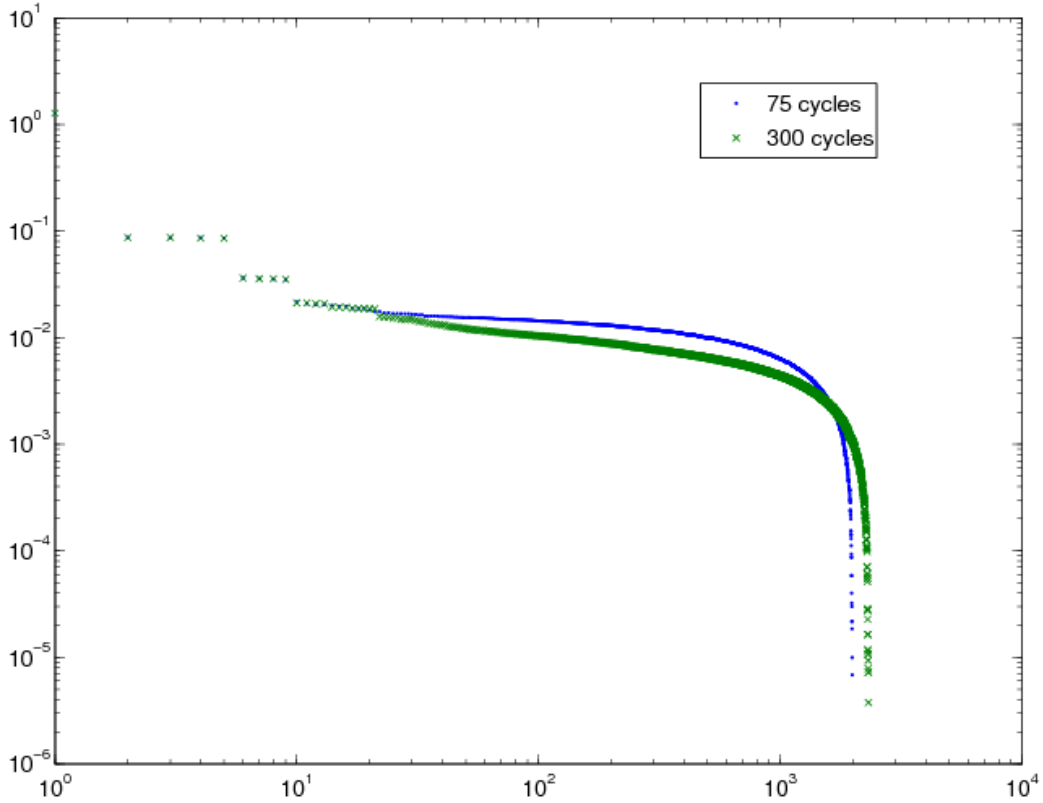


Fig. D.3. Real part of eigenvalue spectrum for infinite lattice of 2.1% enriched 17z17 assembly from 2D PWR problem. Fission matrix tallied for cycles 4-75 and 4-300, batch size of 500 k. 68x68x1 spatial mesh.

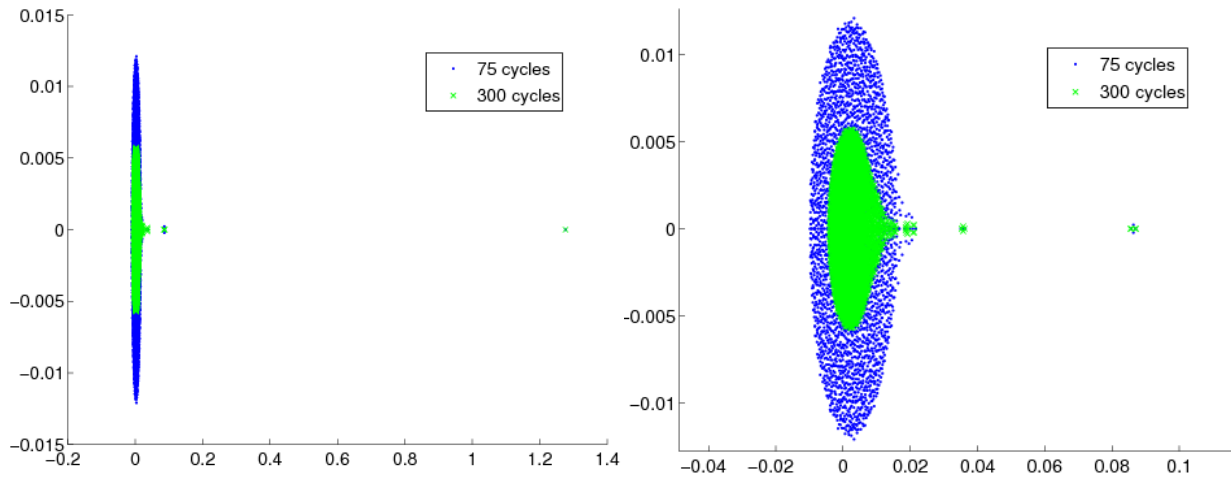


Fig. D.4. Eigenvalue spectrum on complex plane (two scales) for infinite lattice of 2.1% enriched 17z17 assembly from 2D PWR problem. Fission matrix tallied for cycles 4-75 and 4-300, batch size of 500 k. 68x68x1 spatial mesh.

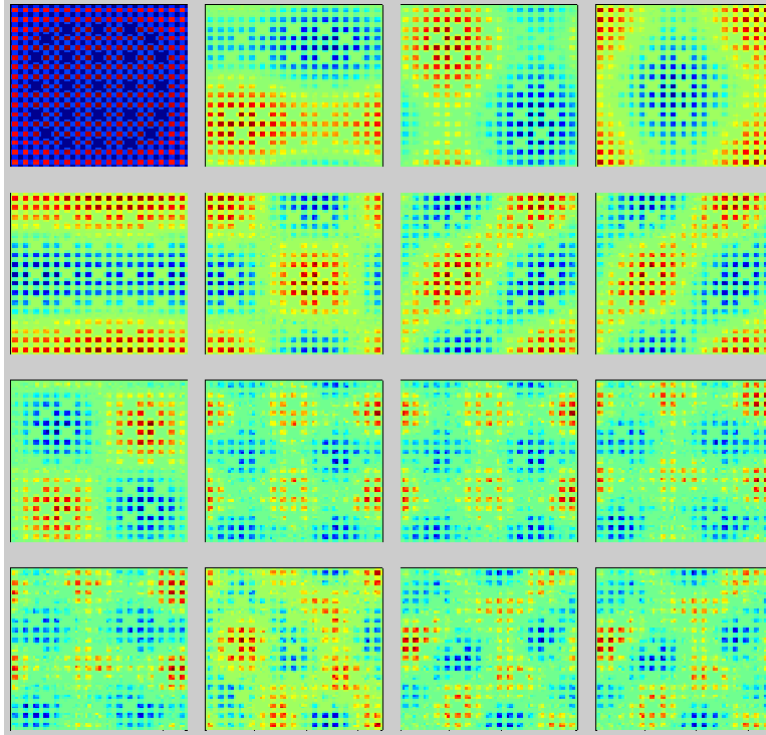


Fig. D.5. Real part of first 16 eigenmodes for infinite lattice of 2.1% enriched 17z17 assembly from 2D PWR problem. Fission matrix tallied for cycles 4-300, batch size of 500 k. 68x68x1 spatial mesh.

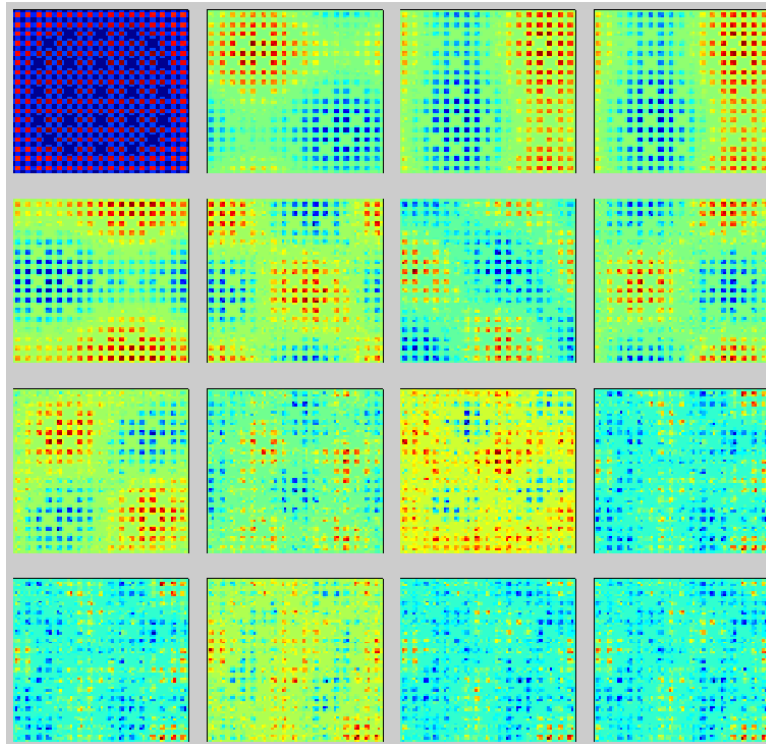


Fig. D.6. Real part of first 16 eigenmodes for infinite lattice of 2.1% enriched 17z17 assembly from 2D PWR problem. Fission matrix tallied for cycles 4-75, batch size of 500 k. 68x68x1 spatial mesh.

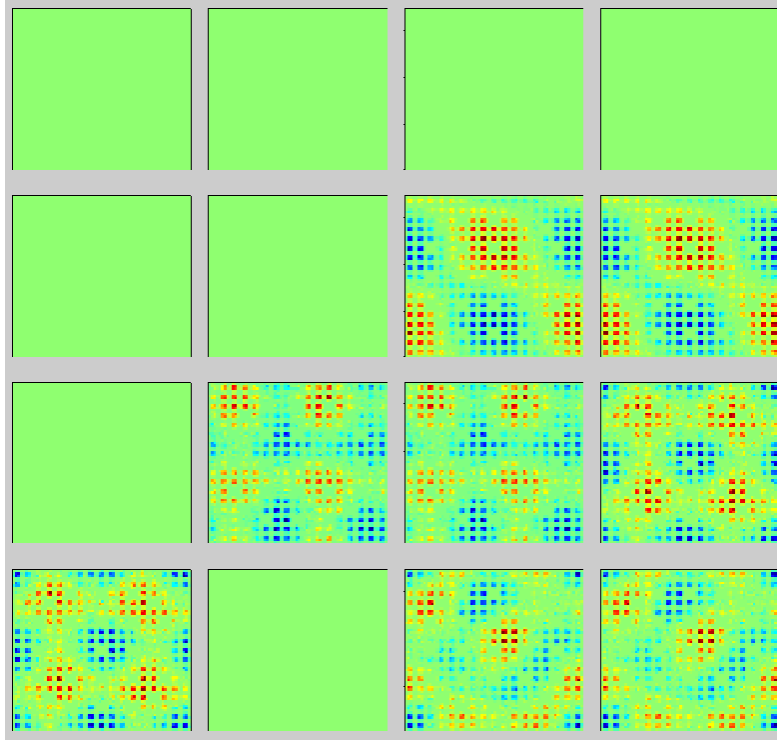


Fig. D.7. Imaginary part of first 16 eigenmodes for infinite lattice of 2.1% enriched 17z17 assembly from 2D PWR problem. Fission matrix tallied for cycles 4-300, batch size of 500 k. 68x68x1 spatial mesh.

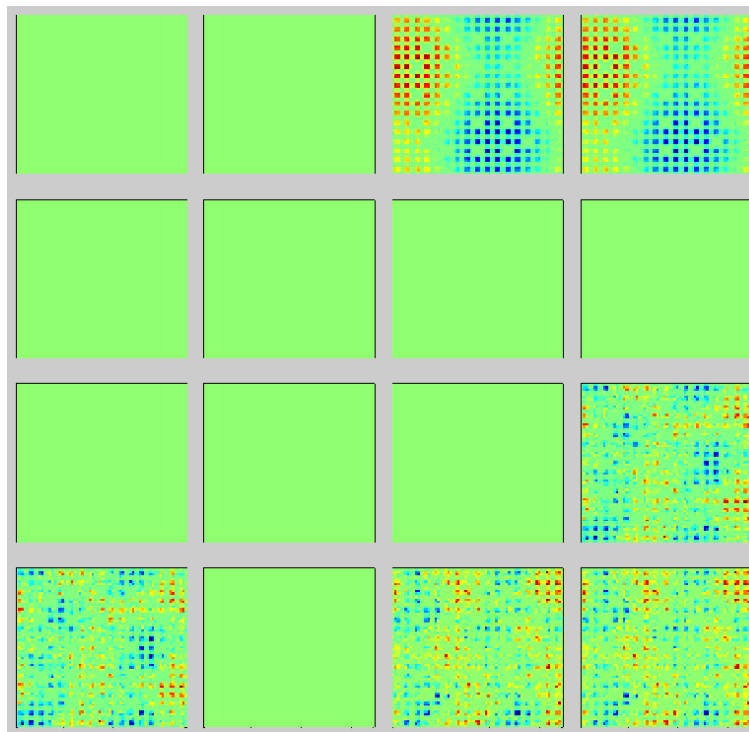


Fig. D.8. Imaginary part of first 16 eigenmodes for infinite lattice of 2.1% enriched 17z17 assembly from 2D PWR problem. Fission matrix tallied for cycles 4-75, batch size of 500 k. 68x68x1 spatial mesh.